Leptospiral lipopolysaccharide dampens inflammation through upregulation of autophagy adaptor p62 and NRF2 signaling in macrophages

Delphine Bonhomme [1], Ignacio Santecchia [1], Pedro Escoll [2], Frédérique Vernel-Pauillac [1], Ivo G. Boneca [1] & Catherine Werts [1*]

[1] Institut Pasteur, Université Paris Cité, CNRS UMR6047, INSERM U1306, Unité de Biologie et Génétique de la Paroi Bactérienne, Paris, France

[2] Institut Pasteur, Université Paris Cité, CNRS UMR6047, Unité Biologie des Bactéries Intracellulaires, Paris, France

[*] corresponding author cwerts@pasteur.fr

ABSTRACT

Leptospira interrogans are pathogenic bacteria responsible for leptospirosis, a worldwide neglected zoonosis affecting yearly 1 million people. All vertebrates can be infected by leptospires. Some species like humans are susceptible to the disease whereas rodents such as mice are resistant and can even become asymptomatic renal carriers. Leptospires have been shown to avoid the activation of some innate immune receptors of the Toll-like receptors (TLRs) and NOD-like receptors families through their atypical microbe associated molecular patterns, and to escape some phagocyte functions. Autophagy is an essential nutrient-recycling cellular mechanism that is also crucial to clear invasive pathogens and is one of the many antimicrobial mechanisms that may be subverted upon bacterial infection. Here we showed that leptospires reduced the quantity of autophagosomes in murine and human macrophages. Moreover, leptospires infection induced a time-dependent specific accumulation of the autophagy adaptor p62 in puncta-like structures. Interestingly, we showed that these effects were not associated with an active leptospiral mechanism but were mediated by the recognition of the atypical leptospiral lipopolysaccharide (LPS) through TLR4 and TLR2. Moreover, we demonstrate in murine macrophages that leptospires induced, *via* p62 accumulation, the nuclear translocation of transcription factor NRF2, consequently triggering the retro-amplification of the p62/NRF2 axis. Finally, inhibition of p62/NRF2 signaling led to increased cytokines transcription and secretion. Overall, this suggests that the p62/NRF2 axis induced by leptospires contributes to dampening inflammation. These findings highlight a novel escape mechanism of leptospires, potentially participating in the stealthiness of the infection.

AUTHOR SUMMARY

Leptospira interrogans are pathogenic bacteria responsible for leptospirosis, a worldwide neglected zoonosis. Some species like humans may suffer from severe disease whereas rodents such as mice are asymptomatic renal carriers. Leptospires have been shown to escape different innate immune receptors of the host immune defenses, and largely escape phagocytosis. Autophagy is a host cell mechanism essential for nutrient-recycling but also crucial to fight and clear intracellular pathogens. Here we show by Western blot and automated microscopy, that infection with leptospires in human and murine macrophages did not trigger autophagy, although it triggered the specific accumulation of the autophagic adaptor p62. Interestingly, we show in murine macrophages that leptospiral infection also activated the nuclear translocation of the transcription factor NRF2. These effects were recapitulated with inactivated bacteria or using the leptospiral lipopolysaccharide (LPS). Finally, we show using RNA interference that inhibiting p62/NRF2 signaling led to increased inflammation. Overall, this suggests that the p62/NRF2 axis induced by the leptospiral LPS contributes to limiting the inflammation in macrophages. These findings highlight a novel mechanism of *Leptospira*, potentially contributing to their stealthiness.

45 **INTRODUCTION**

46 *Leptospira interrogans* are spirochete bacteria and the causative agent of leptospirosis, a
47 worldwide neglected zoonosis that is currently reemerging because of climate change and causes around
48 60 000 deaths *per* year worldwide [1] Although all vertebrates can be infected by leptospires, they do
49 not all present the same symptoms and susceptibility to the disease [2]. Humans as sensitive hosts may
50 suffer from acute leptospirosis ranging from flu-like symptoms to potential multi-organ failure in 5-10%
51 cases [1]. On the other hand, rodents such as mice and rats are resistant to acute illness and get
52 chronically colonized upon infection [3]. Leptospires reach the proximal tubules in the kidneys and
53 establish a stable colonization that leads to their excretion in the urine throughout the life of the animal,
54 contributing to the spread of the zoonosis [3, 4].

55 The host immune defense relies on humoral and cellular components, such as the complement system,
56 immunoglobulins, and phagocytes that patrol to fight microbes. Activation of immune cells such as
57 macrophages are mediated by the sensing of microbial associated molecular patterns (MAMPs) by
58 pattern recognition receptors (PRRs). Leptospires possess numerous lipoproteins, conferring them the
59 ability to potently activate Toll-Like receptor 2 (TLR2) [5, 6]. However, they are stealth pathogens and
60 escape recognition by several other PRRs through unique mechanisms. Our group showed that the
61 leptospiral peptidoglycan escapes NOD receptors recognition by binding to LipL21, one of the
62 numerous leptospiral lipoproteins [7]. We also showed that the leptospiral endoflagella escapes
63 recognition by TLR5 [8]. Furthermore, previous studies on the leptospiral lipopolysaccharide (LPS), a
64 virulence factor [9], revealed that the lipid A (lipidic anchor) possesses structural peculiarities [10] and
65 that it does not activate the human TLR4 whereas it activates the murine TLR4. However, we recently
66 showed that the recognition of the leptospiral LPS in murine macrophages is only partial, because the
67 LPS escapes TLR4 endocytosis and subsequent activation of the TLR4-TRIF pathway [11]. We further
68 demonstrated that the leptospiral LPS activates TLR2 [5], presumably through copurified lipoproteins
69 such as LipL32 (the major leptospiral lipoprotein). On the other hand, our group also showed that
70 leptospires activate the NOD-Like Receptors Pyrin 3 (NLRP) inflammasome and trigger IL1β
71 production [12].

72 In addition to escaping recognition by several PRRs, leptospires also escape phagocytes' functions.
73 Indeed, although leptospires are mostly extracellular bacteria, we reported that leptospires can be found
74 within macrophages without intracellular replication, and that they evade killing by the classical
75 microbicidal mechanisms such as xenophagy [13]. Autophagy is an essential mechanism allowing
76 nutrient recycling upon starvation. Recently, xenophagy arose as a specific form of autophagy
77 promoting the degradation of intracellular pathogens and dampening inflammation [14, 15]. Xenophagy
78 has been shown essential to clear intracellular bacteria, such as *Mycobacterium tuberculosis*,
79 *Shigella flexneri* and *Salmonella typhimurium* [16-18].

80 Autophagy induction is a tightly regulated process: upon stress, class III phosphoinositide
81 3-kinase (PI3K) complex (VSP34, Beclin-1, Atg14) promotes the nucleation of a double membrane
82 called autophagophore [19]. In addition, ULK1/2 phosphorylates Atg13 to form the initiation complex
83 [19]. The expansion of the phagophore is then possible *via* the Atg protein conjugation system [20].
84 Finally, the LC3 conjugation system is required to promote complete autophagosome formation. After
85 translation, pro-LC3 proteins get cleaved (22 amino acids in C-ter) by protease Atg4 producing LC3-I.
86 In turn, LC3-I gets conjugated by Atg7 (E1-like ligase) [21] and Atg3 that promote the addition of a
87 phosphatidylethanolamine (PE) group [22]. The resulting LC3-II localizes on the membrane of the
88 phagophore promoting its maturation in an autophagosome [23] and its fusion with lysosomes, hence
89 leading to cargo degradation by lysosomal enzymes such as cathepsins. Although LC3-II of the inner
90 leaflet will be degraded, LC3-II present in the outer leaflet will be recycled by Atg4, *via* de-lipidation
91 and return to the LC3-I form [21]. Consequently, LC3-II turnover has been proposed as a good way to
92 monitor autophagy [24].

93 Upon infection, several intracellular and extracellular immune signaling pathways can lead to
94 autophagy induction. Toll-Like Receptors (TLRs) signaling facilitates autophagy through interaction of
95 MyD88 complexes with Beclin-1 of the nucleation complex [15]. Furthermore, LPS recognition by
96 TLR4 has been shown to be a potent activator of autophagy, *via* the endosomal TRIF pathway [25].
97 Other studies also demonstrated that NOD1 and NOD2 induce autophagy [26]. Given that leptospires
98 escape both NODs and TLR4-TRIF pathways [7, 11], our study aimed to decipher the interplay between
99 *L. interrogans* and the autophagy machinery of mouse macrophages. Therefore, we assessed autophagy
100 by monitoring LC3-II, and autophagy adaptors, namely p62. Then, considering the importance of
101 bacterial LPS in autophagy modulation [25], we investigated the potential role of the leptospiral LPS in
102 autophagy modulation.

103 RESULTS

104 *L. interrogans* reduces the quantity of autophagosomes in macrophages

105 First, to assess the potential induction of autophagy by leptospires, we infected C57BL/6 mice with
106 *L. interrogans* serovar Manilae (one of the most pathogenic serotypes) strain MFLum1 [4]. We injected
107 intraperitoneally 5 x 10^7 leptospires/mouse and assessed LC3 levels in peritoneal cells by Western blot
108 4 h post-infection. Our results showed that leptospires did not trigger an increase in LC3-II levels, unlike
109 injection of positive controls for autophagy induction: a mix of muropeptides, agonists of NOD1 and
110 NOD2, or rapamycin (**Fig 1A**). Then, we infected bone marrow derived macrophages (BMDMs) *in vitro*
111 with the same strain and monitored LC3-II 24 h post-infection. Here again, in contrast to autophagy
112 induction triggered by rapamycin, we observed no increase in LC3-II after *Leptospira* infection (**Fig 1B**).
113 The same observation was made upon stimulation with heat-killed (HK) leptospires (**Fig 1B**).

114 Furthermore, to address autophagy induction in cells from other vertebrate hosts, we infected human
115 THP1 stably transfected with CD14 (hereafter THP1-CD14) with *L. interrogans* and monitored LC3-II
116 by WB. Our results showed no accumulation of LC3-II after 4 h infection (**Fig S1**). Overall, these data
117 showed that leptospires did not trigger autophagy in macrophages.

118 Second, to address potential modulation of the autophagy flux upon infection, we infected BMDMs with
119 *L. interrogans* and then treated the cells prior to collection with Bafilomycin A1 (BafA1). BafA1
120 inhibits the fusion with lysosomes and arrests autophagy before degradation of cargo, including LC3-II,
121 allowing the accumulation of autophagosomes and consequent analysis of the overall flux. Our results
122 showed that there was an expected accumulation of LC3-II in BafA1 treated cells, but no major
123 difference with or without infection, suggesting that leptospires do not alter the autophagy flux **(Fig 1C)**.
124 To ensure that infection with leptospires did not modulate autophagy at earlier time points, we then
125 performed kinetics analyses of LC3-II. Interestingly, we observed a slight yet robust time-dependent
126 reduction of LC3-II levels 4 h and 24 h post-infection of BMDMs with *L. interrogans*, as evidenced by
127 Western blot and their quantifications (**Fig 1D, lower panel**). Many bacteria interfere actively with
128 autophagy functions via effectors or RNA interference [17, 27-32]. We therefore analyzed BMDMs
129 after stimulation with HK leptospires and we observed similar LC3-II decrease over time (**Fig 1D, right**
130 **panel**), excluding an active mechanism for LC3-II downregulation. To decipher the origin of LC3-II
131 decrease upon infection, we infected BMDMs and analyzed LC3 mRNA levels by RT-qPCR 24 h post-
132 infection. Our results showed that LC3 was not transcriptionally regulated upon infection with
133 leptospires (**Fig 1E**), suggesting a post-transcriptional regulatory mechanism.

134 Last, to confirm this paradoxical LC3-II decrease despite no flux alteration upon infection, we used
135 RAW-mLC3-DiFluo reporter cell line to specifically monitor autophagosomes and autolysosomes
136 formation. These macrophages are stably transfected with LC3 tagged with tandem GFP-RFP. Both
137 GFP and RFP fluoresce under basal conditions and when LC3 is embedded in the autophagosome
138 membrane. However, when autophagosomes become autolysosomes, acidification of the environment
139 quenches GFP fluorescence, and only RFP fluorescence remains. Using High-Content (HC) automated
140 microscopy, we analyzed these cells 4 h post-infection with *L. interrogans*. Our results showed that both
141 autophagosomes (RFP+GFP) and autolysosomes (RFP) were visible in the non-infected cells, and in the
142 starved cells (EBSS) (**Fig 1F, white arrows**). Interestingly, and consistent with the Western blots results,
143 we observed a decrease of the overall LC3-RFP fluorescence intensity upon infection as quantified at
144 4 h post-infection (**Fig 1G**). Unexpecttedly, we found by quantification of the number of
145 autophagosomes and autolysosomes that leptospires triggered a decrease in autophagosome number,
146 without altering the maturation to autolysosomes (**Fig 1G**). Here again, these results confirmed that
147 leptospires did not block the autophagy flux while reducing the LC3-II autophagosomes structures.

149 ***L. interrogans* induces specific accumulation of autophagy adaptor p62 in puncta-like structures**

150 The adaptor proteins, such as Sequestosome 1 (SQSTM1, also known as p62), Nuclear Dot Protein 52
151 (NDP52) and optineurin (OPTN) [17, 33-36] are important players of xenophagy that allow selective
152 bridging between the bacterial cargo and the autophagosome. The levels of these adaptors in the cells
153 are regulated by autophagy: they are constitutively degraded upon lysosome / autophagosome fusion.
154 Considering the LC3-II decrease induced by *L. interrogans*, we then addressed the consequences of the
155 infection on the autophagy adaptors. We infected BMDMs with *L. interrogans* serovar Manilae strain
156 MFLum1 and analyzed by Western blots the levels of the different adaptors. Strickingly, we observed
157 a time-dependent accumulation of p62 upon infection (**Fig 2A**). We confirmed this phenotype upon
158 infection of BMDMs with two other strains from pathogenic serotypes of *L. interrogans*: serovar
159 Copenhageni strain Fiocruz L1-130 and serovar Icterohaemorrhagiae strain Verdun, and with the
160 saprophytic *Leptospira biflexa* serovar Patoc strain Patoc I (**Fig 2B**). Such accumulation of the adaptor
161 p62 could have been non-specifically associated with the reduction of autophagosomes. However, while
162 performing infection of RAW264.7 cells, we observed no difference in the levels of other adaptors
163 OPTN and NDP52 upon infection (**Fig S2A**). We concluded that *L. interrogans* triggered specific
164 accumulation of p62 in murine BMDMs.

165 To investigate the specific mechanism of p62 accumulation triggered by leptospires, we analyzed the
166 transcriptional regulation of p62 upon infection by RT-qPCR. In BMDMs infected with *L. interrogans*,
167 we observed a significant upregulation of p62 mRNA 24 h post-infection (**Fig 2C**). This corroborated
168 the idea that p62 accumulation is not only mediated by autophagy downregulation. Furthermore, we
169 also analyzed infected BMDMs by fluorescence microscopy and we observed that, 4 h post-infection,
170 p62 accumulated in puncta-like structures (**Fig 2D**). The kinetics of these p62 puncta formation were
171 further characterized using automated HC confocal microscopy. Upon infection of RAW264.7 cells by
172 *L. interrogans*, we quantified the number of p62 puncta *per* cell, as well as the percentage of cells with
173 p62 puncta. Results showed time-dependent increase of both p62 puncta *per* cell and percentage of
174 positive cells and showed around 80% of cells positive for p62 with an average of 6 puncta *per* cell 24 h
175 post-infection (**Fig 2E**). Similar analyses were performed after infection with *L. biflexa*, confirming a
176 higher p62 puncta formation with the saprophytic strain, compared to the pathogenic Manilae
177 (**Fig S2B**). Such findings were confirmed by single cell analysis of RAW264.7 cells infected with
178 *L. interrogans*, that showed an average of 5-10 puncta *per* cell with some macrophages containing up
179 to 60 p62 puncta (**Fig 2F**). Of note, BafA1 that prevents the acidification of lysosomes and consequently
180 blocks autophagy flux also led to p62 accumulation, but to a much lower extent than infection with
181 leptospires (**Fig 2E and 2F**).

182 Finally, considering the host species-specificity of different escape mechanisms triggered by leptospires,
183 we also addressed in human cells the effect of infection on p62. Therefore, we infected THP1-CD14

184 cells with *L. interrogans* serovar Manilae strain MFLum1. We also observed a specific p62
185 accumulation and no NDP52 accumulation after infection with leptospires (**Fig S2C**), suggesting a
186 conserved mechanism in human and murine macrophages.

187 **Autophagy modulation is mediated by TLR2/TLR4**

188 Considering that leptospires did not reduce LC3-II levels through an active mechanism, we then
189 addressed the role of PRRs in autophagy modulation. Since leptospires are potent agonists of TLR2 and
190 signal through TLR4-MyD88 in murine cells [11], we analyzed autophagy modulation in macrophages
191 lacking both TLR2 and TLR4. To do so, we infected wild-type (WT) and TLR2/TLR4 double knock-out
192 (TLR2/4 dko) BMDMs with *L. interrogans*. After 24 h of infection, we assessed by Western blot the
193 levels of LC3-II and p62. Our results showed that, in contrast to WT cells, there was no reduction in
194 LC3-II and no accumulation of p62 in TLR2/4 dko BMDMs (**Fig 3A**), suggesting that autophagy
195 modulation by leptospires is mediated by these two receptors. To further confirm such results, we also
196 infected WT and MyD88/TRIF dko macrophages, that lack both adaptors for TLRs signaling. Here
197 again, we observed no accumulation of p62 in MyD88/TRIF BMDMs compared with the WT BMDMs
198 (**Fig 3B**).

199 Finally, we investigated the role of TLR2/TLR4 in the specific accumulation of p62. We first analyzed
200 infected BMDMs by RT-qPCR and observed that the increase in p62 mRNA levels observed in WT
201 BMDMs was abolished in TLR2/4 dko BMDMs (**Fig 3C**). Furthermore, we performed single cell
202 analysis of p62 puncta formation in WT, TLR2/4 dko and MyD88/TRIF dko BMDMs upon 24 h
203 infection by three serotypes of *L. interrogans* (serovar Manilae strain L495, serovar Copenhageni strain
204 Fiocruz L1-130 and serovar Icterohaemorrhagiae strain Verdun). Our results showed that the number of
205 p62 puncta *per* cell was greatly reduced in TLR2/TLR4 dko cells and almost completely abolished in
206 MyD88/TRIF dko cells (**Fig 3D**), which may suggest the involvement of other TLRs than TLR2 and
207 TLR4s in the leptospiral p62 upregulation.

208 Given that leptospires modulate autophagy in a TLR2/TLR4 dependent manner, we finally addressed
209 the potential role of inflammasome in autophagy dampening. Indeed, leptospires have been shown to
210 activate NLRP3 in a TLR2/TLR4-dependent manner [12], and NLRPs inflammasomes have been
211 shown to modulate autophagy [37-40]. We therefore stimulated BMDMs with both live and heat-killed
212 leptospires in presence or absence of glibenclamide, a NLRP3 inhibitor. We first confirmed the
213 efficiency of the treatment by measuring IL1β production after 24 h, as a readout for inflammasome
214 activation. Our result showed that IL1β was produced upon infection by leptospires, but reduced in
215 presence of glibenclamide, confirming that glibenclamide inhibited NLRP3 (**Fig S3A**). We then
216 analyzed by Western blot the levels of LC3-II, and we observed a reduction of LC3-II upon infection
217 with either live or heat-killed leptospires in both control and glibenclamide treated cells (**Fig S3B**). This

218 suggests that the modulation of autophagy by leptospires, although TLR2/TLR4 dependent, is not
219 mediated by activation of NLRP3 inflammasome.

220 **p62 accumulation is mediated by the leptospiral LPS**

221 With the predominant role of TLR2 and TLR4 in autophagy modulation, and transcriptional regulation
222 of p62, we then hypothesized that these effects could be induced by the leptospiral LPS. To address the
223 role of the leptospiral LPS in the p62 accumulation phenotype, we first infected BMDMs with both
224 heat-killed leptospires (recapitulating MAMPs) and purified leptospiral LPS. Western blot analyses
225 showed that p62 got accumulated in a time-dependent manner in response to both heat-killed leptospires
226 and also 24 h post-stimulation with their LPS (**Fig 4A**). We further characterized by HC microscopy the
227 kinetics of p62 puncta formation in BMDMs after incubation with live, heat-killed *L. interrogans*
228 serovar Manilae strain L495 and purified LPS. Results indicated that LPS stimulation induced the exact
229 same p62 puncta formation than the one observed with bacteria (**Fig 4B**). Next, we also analyzed
230 BMDMs at the single cell level 24 h post-infection. Here again, HK leptospires or the leptospiral LPS
231 were sufficient to recapitulate p62 puncta formation in cells (**Fig 4C**). Overall, our results showed that
232 p62 accumulation was mediated by the leptospiral LPS.

233 **Leptospiral LPS also triggers translocation of NRF2 transcription factor**

234 When autophagy adaptors accumulate in cell (in the absence of functional autophagy or because of
235 specific upregulation), stress pathways are induced. For instance, p62 accumulation has been shown to
236 induce translocation of stress-responsive nuclear factor erythroid 2-related factor 2 (NRF2) [41-43].
237 Subsequently, NRF2 triggers antioxidant and anti-apoptotic programs [41, 42], and promotes p62
238 upregulation, creating a loop that counteracts stress in autophagy-deficient conditions [41]. We therefore
239 infected BMDMs with *L. interrogans* serovar Manilae strain L495 and analyzed NRF2 by
240 immunofluorescence 4 h post-infection. Results showed that NRF2 staining was barely visible in the
241 non-infected conditions, whereas NRF2 was visible in the nucleus of cells upon infection (**Fig 5A**). This
242 suggests that leptospires triggered NRF2 translocation in murine macrophages. Interestingly, we also
243 observed that not all macrophages seem activated to the same extent (**Fig 5A**). Then, we decided to
244 perform single cell analysis of NRF2 fluorescence intensity in the nucleus of cells infected with three
245 different serovars of *L. interrogans*. Similarly, upon infection, the levels of NRF2 fluorescence in the
246 nucleus increased (**Fig 5B**). Next, we calculated the ratio of NRF2 intensities [nucleus/cytoplasm] and
247 estimated that cells positive for NRF2 had a ratio > 1.4. We then plotted the percentage of cells with
248 NRF2 ratio superior to 1.4 and observed that up to 60% of cells were positive after 4 h of infection
249 (**Fig 5C**). Finally, we addressed the role of the leptospiral LPS and performed similar analyses on
250 BMDMs stimulated for 4 h with either live, heat-killed leptospires or their purified LPS. All conditions

251 triggered similar NRF2 translocation (**Fig 5D and 5E**), suggesting that the leptospiral LPS is responsible
252 for NRF2 activation.

253 **p62 and NRF2 constitute a retro-activation loop upon infection with *L. interrogans***

254 Consequently to p62 accumulation and NRF2 translocation upon infection with *L. interrogans*, we
255 investigated the potential regulation mechanisms between these two phenotypes. Thus, we performed
256 small-interfering RNA (siRNA) transfection in BMDMs to knock-down specifically p62 or NRF2. We
257 then infected the transfected BMDMs and analyzed NRF2 and p62 4 h post-infection by HC microscopy.
258 First, we analyzed the NRF2 ratio [nucleus/cytoplasm] during p62 knocking-down. Our results showed
259 that NRF2 ratio was lower in p62 siRNA condition (**Fig 6A**). Absence of p62 was confirmed and
260 quantified by confocal microscopy (**Fig 6B**). Conversely, we then analyzed p62 puncta formation upon
261 NRF2 siRNA treatment. Our results showed that p62 puncta formation was altered in NRF2 siRNA
262 conditions (**Fig 6C**). Similalrly, NRF2 knocked-down was confirmed and quantified (**Fig 6D**). Overall,
263 these results showed that p62 contributed to NRF2 translocation, and that, in turn, NRF2 regulated p62
264 puncta formation, suggesting that p62 and NRF2 are in a retro-activation loop upon infection by
265 *L. interrogans*.

266 To further characterize the involvement of NRF2 in p62 retro-activation, we analyzed BMDMs
267 transfected with NRF2 siRNA and infected with *L. interrogans* by Western blot and RT-qPCR 24 h
268 post-infection, allowing us to measure both the protein and mRNA levels of p62. Interestingly, we
269 observed that NRF2 silencing prevented p62 protein accumulation (**Fig 6E**) but also reduced mRNA
270 upregulation (**Fig 6F**), suggesting that NRF2 contributes transcriptionally to p62 retro-activation.

271 **NRF2 translocation prevents inflammation upon infection**

272 NRF2 is a stress response transcription factor that promotes antioxidant and antiapoptotic programs
273 upon activation [41, 42]. Therefore, we first monitored the transcription of targets genes involved in
274 fighting oxidative stress in macrophages in response to infection. We infected BMDMs with
275 *L. interrogans* and analyzed by RT-qPCR the levels of gluthatione S-reductase and catalase mRNA at
276 4 h and 24 h post-infection. Surprisingly, we observed no upregulation of these transcripts (**Fig S4A**
277 **and S4B**), suggesting that no antioxidant program is activated upon infection with *L. interrogans*.

278 Interestingly, NRF2 was shown to also have repressor functions and to dampen inflammation by
279 inhibiting the transcription of cytokines [44, 45], hence conferring resistance to inflammatory disease
280 such as sepsis [44]. We therefore investigated the role of NRF2 translocation in inflammation upon
281 infection by leptospires. We transfected RAW624.7 cells with siRNA targeted against NRF2 and then
282 infected them with *L. interrogans*. First, we observed a decrease in macrophage viability upon infection
283 of NRF2-silenced cells (**Fig 7A, left panel**), as expected considering that NRF2 is known to prevent

284 cell death. Interestingly, this enhanced loss of viability was not associated with lactate dehydrogenase
285 (LDH) release from the cytosol, illustrating that no membrane damage or cell lysis was occurring
286 (**Fig 7A, right panel**). We then analyzed the mRNA levels of several cytokines and enzymes, namely
287 iNOS (nitric oxide inducible synthase), IL6, TNF and IL10. Upon infection, all mRNA levels were
288 higher in NRF2-silenced cells than in control cells (**Fig 7B**), suggesting that NRF2 does play a role in
289 repressing the expression of inflammatory targets. Finally, to address whether this transcriptional
290 regulation was strong enough to alter cytokines levels, we analyzed nitric oxide (NO), IL6, TNF and
291 IL10 production in cell supernatant. Consistent with the mRNA analyses, we observed higher NO, IL6
292 and TNF upon infection of NRF2-silenced RAW264.7 (**Fig 7C**). Interestingly, IL10 levels were not
293 modulated in NRF2-silenced cells. All these findings were even more striking when normalizing the
294 cytokines production with the cell viability (**Fig 7C, grey area**). Overall, NRF2 played a repressor role
295 to dampen NO, TNF and IL6 production in mouse macrophages upon infection with *L. interrogans*.

296 **DISCUSSION**

297 Our results showed that *L. interrogans* does not induce autophagy in macrophages either
298 *in vivo* in mice or *in vitro* in murine and human cells. These findings are consistent with previous studies
299 from our laboratory showing that leptospires escape NOD1/NOD2 [7] and TLR4-TRIF [11] activation,
300 since both pathways have been described as autophagy inducers [25, 26]. Furthermore, infection with
301 leptospires unexpectedly triggered a slight reduction of the number of autophagosomes, without
302 alteration of the autophagy flux. To this date, we do not know what the functional consequences of such
303 downregulation are, warranting further investigations. Interestingly, using heat-killed leptospires we
304 observed similar results, excluding a potential active mechanism. We conclude that the leptospires
305 behave differently from other pathogenic bacteria such as *Legionella pneumophila, Shigella flexneri* or
306 *Listeria monocytogenes* for which autophagy modulation is mediated by effector proteins, namely RavZ,
307 IcsB and ActA respectively [31, 32]. An effector-independent mechanism is even more consistent with
308 the fact that leptospires do not possess traditional secretion systems (SS) such as type-III SS or
309 type-IV SS. Indeed, only the presence of an incomplete type-II SS has been identified in *Leptospira*
310 species [46]. Consistently, a study revealed that 59% of the pathogen-specific leptospiral genes have
311 unknown functions, strongly suggesting that the leptospiral virulence may rely on unique and novel
312 mechanisms [3]. Our results further showed that the modulation of autophagy was induced by leptospiral
313 LPS signaling through TLR2/TLR4. The unique leptospiral LPS, the best characterized virulence
314 factor [9], plays an important role in leptospiral host-pathogen interactions. Indeed, we previously
315 showed that leptospiral LPS avoids human TLR4 and mouse TLR4-TRIF activation. Recently, through
316 the atypical structures of its lipid A and O antigen [11, 47, 48], LPS has also been shown to prevent cell
317 death by pyroptosis. Therefore, it was not surprising to attribute the autophagy modulation phenotype
318 to leptospiral LPS. Interestingly, the LPS of *L. biflexa* was shown to be a more potent TLR4 agonist

319 [11], potentially explaining the stronger p62 accumulation observed after infection with the saprophytic
320 strain.

321 TLRs signaling has classically been associated to autophagy induction, mainly through TLR4-
322 TRIF [25] but also *via* TLR2, TLR3, TLR4, TLR5 and TLR7 signaling with MyD88 [15]. However,
323 consistent with our results, some studies also reported that TLRs signaling can also block autophagy.
324 For instance, LPS signaling downregulates autophagy in non-inflammatory dendritic cells (DCs) [49]
325 and in microglial cells [50], evidencing the complexity of the autophagy/TLR interplay. In DCs, TLR4
326 has been associated with mTOR activation, hence reducing the autophagy flux [49]. Whether this
327 mechanism could also be used by leptospires in macrophages remains to be answered. In addition,
328 leptospires have been shown to induce NLRP3 in a TLR2/TLR4-dependent manner [12]. Although the
329 interplay between NLRP3 and autophagy is unclear, several studies reported that NLRP3 can dampen
330 autophagy [37-40]. Therefore, we hypothesized that *Leptospira*-induced NLRP3 could modulate
331 autophagy. However, our results suggest that the NLRP3 does not contribute to the autophagy
332 modulation.

333 A consequence of autophagy downregulation is the accumulation of a central player of the
334 autophagy pathway, the p62/SQSTM-1 adaptor [43]. This protein has been shown to accumulate *via*
335 TLRs signaling [51], most likely through NFκB-mediated transcriptional regulation. Our results showed
336 that TLR2/TLR4 control the accumulation of p62 upon infection by leptospires. Nevertheless, we cannot
337 differentiate a direct mechanism (NFκB) from an indirect one (autophagy dysregulation). Our data
338 showing that p62 is transcriptionally regulated led us to favor the first hypothesis. Moreover, the levels
339 of p62 upon infection are higher than after BafA1 treatment, suggesting that the accumulation of p62 is
340 mostly independent of the slight autophagy downregulation induced by leptospires.

341 The TLRs-induced accumulation of p62 has been shown to trigger the translocation of the
342 transcription factor NRF2 [51]. Under physiological conditions, NRF2 is classically targeted for
343 degradation by the proteasome *via* interaction with its inhibitor Keap1 [43, 52]. The accumulation and
344 direct binding of p62 to Keap1, leads to its sequestration and subsequent release from NRF2, which then
345 can translocate in the nucleus [41-43, 52]. Our results confirmed that p62 induces translocation of NRF2
346 upon infection with leptospires. Other microbes such as Epstein-Barr virus (EBV) or parasite
347 *Leshmania major* have been shown to activate the p62/NRF2 axis [53, 54], hence showing an important
348 role of NRF2 in response to pathogens. However, to date, the role of NRF2 translocation in response to
349 pathogens remains unclear.

350 We then illustrated that the retro-activation loop between p62 and NRF2, described in the
351 literature [41], is activated upon *L. interrogans* infection. Our results showed that p62 accumulation
352 triggered translocation of NRF2 and that in turn, NRF2 contributed to the transcriptional regulation of
353 p62. Interestingly, this loop has few negative regulators, and it is hypothesized that its main regulator

354 would be autophagy, through degradation of p62 [41]. However, considering the lack of autophagy
355 induction upon infection with leptospires, it is not surprising that the loop remains active and that p62
356 puncta did not disappear even at 24 h post-infection. This suggests that leptospires are potent activators
357 of the p62/NRF2 axis in macrophages.

358 NRF2 is involved in numerous pathways including the induction of antioxidant programs [41].
359 We were therefore surprised to observe no modulation in the mRNA levels of antioxidant targets, such
360 as catalase or gluthatione S-reductase, either at 4 h or 24 h post-infection. Of note, pathogenic
361 leptospires are equipped to fight against oxidative stress with inducible catalase, peroxidase, and
362 peroxiredoxin [55]. We therefore hypothesize that leptospires would not benefit from induction of
363 antioxidant program in the host cells. Interestingly, active repression of these NRF2-dependent
364 antioxidant targets was previously shown upon infection with live *Leshmania major* parasite [54, 56]
365 Whether leptospires could also actively prevent upregulation of NRF2 antioxidant targets remains to be
366 addressed.

367 Alternatively, NRF2 has been shown to have transcription inhibition properties. Indeed, in
368 BMDMs, NRF2 was described as an inhibitor of transcription for pro-inflammatory targets such as IL6,
369 IL1β and IL12 [45, 57]. Our results showed that this was also the case upon infection with *L. interrogans*.
370 Accordingly, we did not observe dampening of the anti-inflammatory IL10 upon infection. NRF2
371 inhibits polymerase III recruitment and hence prevents transcription of cytokines in response to
372 stimulation [45]. Consequently, NRF2 was shown to downregulate neutrophils activation and
373 migration [58]. Interestingly, neutrophils are barely observed in tissues of mice and humans infected
374 with leptospires, although they are found in numbers in blood [59, 60]. Whether NRF2 translocation in
375 specific cell type could have a role in this phenotype remains to be studied. NRF2 was also associated
376 to inflammation reduction *via* indirect mechanism relying on STING and type I IFN
377 downregulation [61], which remains to be studied in the case of leptospiral infection.

378 Finally, we showed that accumulation of p62 observed in murine macrophages was conserved
379 in human cells. Although we could not address NRF2 translocation in human cells due to lack of specific
380 antibodies and tools, we may speculate that inflammation dampening could therefore be conserved in
381 human macrophages. Although the functional consequences of this mechanism remain to be addressed,
382 we believe it could play a key role in the discretion of leptospires in hosts, lack of immune cell
383 recruitment and potentially contribute to the establishment of chronic infections.

385 **MATERIALS AND METHODS**

386 ***Leptospira interrogans* cultures.** *Leptospira interrogans* used in this work (serovar Manilae strain
387 L495 and bioluminescent derivative MFLum1 [4], serovar Copenhageni strain Fiocruz L1-130, serovar
388 Icterohaemorragiae strain Verdun) and *Leptospira biflexa* (serovar Patoc strain Patoc I) were grown in
389 Ellinghausen-McCullough-Johnson-Harris (EMJH) medium at 28°C without agitation and diluted
390 weekly, or twice a week for *L. biflexa*, to obtain exponential phase growth culture at the time of
391 experiments. For infection, leptospires cultures were centrifuged (3250 g, 25 min), resuspended in
392 endotoxin-free PBS (Lonza), enumerated using a Petroff-Hauser chamber and bacterial concentration
393 was adjusted accordingly. To inactivate bacteria (thereafter called "heat-killed") leptospires were heated
394 at 56 °C for 30 min with mild agitation. For fluorescent labelling, 10 mL of exponential culture was
395 centrifuged (3250 g, 25 min) and the pellet was resuspended in the same volume of PBS (Lonza) with
396 addition of 10 µM CFSE (Sigma). The bacterial suspension was incubated at room temperature for 30
397 min protected from light and washed 1 time with 20 mL of PBS before counting and infection.

398 **Mice experiments.** Adults male and female mice of the following genotypes in a C57/BL6 background
399 were used: WT (Janvier Labs, Le Genest-Saint-Isle, France); TLR2$^{-/-}$TLR4$^{-/-}$ and MyD88$^{-/-}$/TRIF^{lps2}
400 (both from Institut Pasteur). For peritoneal cavity analyses, mice were injected *via* intraperitoneal route
401 with 5 x 10^7 leptospires/mouse, 30 µg/mouse of rapamycin (Sigma) or 30 µg/mouse of NOD1 agonist
402 (FK156) [62] and NOD2 agonist (MDP, Invivogen) in PBS. Next, 4 h post-infection mice were
403 euthanized, and peritoneal content was recovered as previously described [63]. Briefly, skin was peeled
404 and clamped, followed by the injection of 2 mL of RPMI media. Next an incision was made on the pre-
405 clamped skin to recover the peritoneal content. Peritoneal cells were then used for sample preparation
406 and Western blot analyses, as described below.

407 **Ethic statement.** All protocols were undertaken in compliance with EU Directive 2010/63 EU and the
408 French regulation on the protection of laboratory animals issued on February 1st, 2013. They are part of
409 projects approved by the Institut Pasteur ethics committee for animal experimentation (Comité
410 d'Ethique en Expérimentation Animale CETEA registered under #89) under # HA0036 for the bone
411 marrow cells, and #2014-0049 for the leptospiral infections, which was authorized by the French
412 Ministry of Research, the French Competent Authority under #8562.

413 **Cell culture.** RAW264.7 murine macrophage-like cell line was cultured in complete RPMI containing
414 glutamine (Lonza) and supplemented with 10 % v/v heat-inactivated fetal calf serum (HI-FCS, Gibco),
415 1 mM non-essential amino acids (MEM, Gibco) and 1 mM sodium pyruvate (NaPy, Gibco).
416 RAW-mLC3-DiFluo (Invivogen) autophagy reporter cells stably transfected with LC3-GFP-RFD were
417 cultivated in the same conditions, with the addition of 100 µg/mL zeocin (Invivogen) for efficient
418 selective pressure. All the cells were seeded in 96-, 24-, 12-well plates (TPP) the day before infection at
419 a concentration of 0,3x10^6 cells/mL in 200 µL, 1 mL or 2 mL respectively, in antibiotic-free medium.

420 Human THP-1 monocyte-like cell line, stably transfected with CD14 (THP1-CD14), was culture in
421 complete RPMI, and the cells were differentiated for 48 hours with 20 ng/mL of phorbol 12-myristate
422 13-acetate (PMA, Invivogen) at $1x10^6$ cells/mL. The cells were then washed 3 times with PBS and
423 allowed 24 hours of resting before infection.

424 BMDMs were obtained from different genotypes of C57BL/6 background mice. After euthanasia by
425 cervical dislocation, the head of each bone was removed, and 2 mL of medium were passed through the
426 bones using a 22 G needle to flush out the bone marrow. Bone marrow cells were centrifuged (300 g,
427 7 min) and treated with Red Blood Cell Lysis Buffer (Sigma-Aldrich) for 10 minutes, followed by
428 another centrifugation. The cells were then enumerated, and $5x10^6$ cells were seeded in 100 cm^2 cell
429 culture dishes in 12 mL of complete RPMI supplemented with 10% v/v L929 cell supernatant and 1x
430 PenStrep (Gibco). Cells were incubated at 37 °C, 5 % CO_2. At day 3, 3 mL of the same medium was
431 added. At day 7, the cells were collected by scraping in Cell Dissociation buffer (Gibco), centrifuged,
432 enumerated, and seeded for infection at $1x10^6$ cells/mL.

433 In addition to the infections with *L. interrogans*, other treatments were performed. Starvation was
434 induced in minimum EBSS media (Gibco) after 2 washes to remove complete cell culture media.
435 Autophagy was induced with 500 mM rapamycin (Sigma). For blockage of autophagy flux, 100 nM
436 bafilomycin A1 (BafA1, Sigma-Aldrich) was added to the infected cells 4 h before cell collection and
437 analyses. The inflammasome inhibitor glibenclamide (Thermo Fisher) was added at 25 µM, 30 min
438 before infection. Finally, stimulations by leptospiral LPS were performed by incubating the cells with
439 1 µg/mL of LPS of *L. interrogans* (serovar Manilae strain L495, serovar Copenhageni strain Fiocruz
440 L1-130 or serovar Icterohaemorragiae strain Verdun) extracted from the phenol phase of the hot
441 water/phenol extraction protocol, as we recently reviewed[64].

442 **Immunofluorescence and High Content (HC) microscopy.** For classical IF analyses, cells were
443 seeded in 24-well plate containing 1 cover glass per well (18 mm diameter, # 1.5 thickness, Electron
444 Microscopy Science). After infection, cells were fixed in 4 % v/v *para*-formaldehyde for 10 min,
445 followed by three washes with PBS. Cells were blocked 1 h in PBS with 2.5% w/v bovine serum albumin
446 (BSA) and 2.5 µg/mL anti-CD16-CD32 (FcBlock, Thermo Fisher). Cells were stained after blocking
447 with primary antibodies (**Table 1**) overnight at 4 °C in PBS 1% w/v BSA, 0.05% w/v saponin. Cells
448 were then washed three times with PBS and were incubated with fluorescent secondary antibodies
449 (**Table 1**) and 1µg/mL DAPI in PBS 1% w/v BSA, 0.05% w/v saponin for 1 hour at room temperature.
450 For NRF2 nuclear staining, permeabilization was initially performed by 10 min incubation in PBS 1%
451 w/v BSA, 0.5% v/v Triton X-100 prior to blocking, and saponin was not used. In all cases, cells were
452 washed three times with PBS and image acquisition was performed on Leica SP5 confocal microscope
453 (63x - 1.4 NA, oil immersion). Default settings were used and both UV and argon lasers were used at
454 power between 5-40 %.

455 For HC microscopy analyses, cells were seeded in dark, transparent bottom 96-well plates
456 (Greiner, µClear) at 0,1x10^6 cells/mL. Staining protocols are identical to the ones described above,
457 except for RAW-mLC3-DiFluo cells that were fixed to 10 min in cold ethanol/acetone (1:1) buffer. All
458 cells were then kept in PBS for imaging by Opera Phenix HCS (Perkin Elmer) using confocal settings
459 with a 63X water-immersion objective (NA 1.15). Light source was kept at 20 to 50% power and
460 exposure time was set for each experiment to obtain intensities around 1000-5000. Automated
461 acquisition was launched to acquire a minimum of 500-1000 cells/well in technical triplicates for each
462 experiment. Automated image analysis workflow and puncta quantification was performed using
463 Columbus image data storage and analysis system (PerkinElmer), with the following steps: *(i)* import
464 data; *(ii)* find nuclei with DAPI signal; *(iii)* find cytoplasm with the background of the target protein
465 signal (NRF2 or p62); *(iv)* find spots using method C if relevant (for p62); *(v)* formulate classical outputs:
466 number of p62 puncta, NRF2 intensity in nucleus/cytoplasm; *(vi)* formulate calculated outputs: %p62
467 positive cells, NRF2 ratio, %NRF2 positive cells*; (vii)* save script and run batch analysis and *(viii)* export
468 data.

469 **Table 1.** Antibodies list for immunofluorescence and Western blot analyses

Application*	Target	Clonality**	Conjugated	Host	Dilution	Reference	Supplier
IF	**p62**	mAb	Purified	Rabbit	1:500	ab109012	Abcam
	Rabbit IgG	pAb	AlexaFluor 488	Goat	1:1.000	A-11034	ThermoFisher
IF	**Nrf2**	mAb	Purified	Rat	1:250	#14596	CST
	Rat IgG	pAb	AlexaFluor 647	Goat	1:1.000	A-21247	ThermoFisher
WB	**LC3**	pAb	Purified	Rabbit	1:1.000	L7543	Sigma
	p62	mAb	Purified	Mouse	1:1.000	ab109012	Abcam
	OPTN	pAb	Purified	Rabbit	1:1.000	ab23666	Abcam
	NDP52	pAb	Purified	Rabbit	1:1.000	GTX115378	GeneTex
	Rabbit IgG	pAb	HRP	Goat	1:10.000	7074S	CST

470 * IF: immunofluorescence, WB: Western blot, ** mAb: monoclonal antibody, pAb: polyclonal antibody

471 **SDS-PAGE and Western blot**. For proteins collection and Western blot analyses, cell supernatants
472 were removed, and 1 mL of Cell Dissociation buffer (Gibco) was added and incubated for 5 minutes,
473 followed by scrapping, collection, and centrifugation (400 g, 10 min, 4 °C). The pellets were
474 resuspended in 50 µL of ice-cold RIPA lysis buffer supplemented with 1x complete Mini, EDTA-free
475 proteases inhibition cocktail (Roche). Cells were lysed on ice for 20 min followed by a centrifugation
476 step (12000 g, 40 min, 4 °C) to remove the non-soluble material. Proteins were dosed using the Bradford
477 assay and the samples were denatured in Laemmli buffer (99 °C, 10 min). SDS-PAGE was done using
478 4-15% gradient acrylamide Stain-free gels (BioRad), loaded with 5-10 µg of protein extract *per* lane
479 and gels were run at 100 V in Tris-Glycine-SDS buffer (BioRad). Proteins were visualized using stain

480 free reagent in ChemiDoc (BioRad) with a 5 min exposition time and transferred onto a 0.22 µm PVDF
481 membrane (BioRad) using Mixed MW fast transfer of 1 miniGel (BioRad). The membrane was blocked
482 with 5% BSA in TBS with 0,05% v/v Tween 20 (TBS-T) for 60 minutes at room temperature with mild
483 agitation. The membrane was probed with either anti-LC3 or anti-p62, anti-NDP52, anti-OPTN
484 (**Table.1**) in 5% BSA in TBS-T overnight at 4 °C. The membranes were then washed in TBS-T 3 times
485 for 15 minutes followed by incubation with secondary anti-rabbit IgG HRP-linked (**Table 1**) in 5% BSA
486 in TBS-T for 60 minutes protected from light at room temperature, followed by 3 washes in TBS-T for
487 15 minutes. Blots were revealed using the Clarity reagent (BioRad) with automatic exposure time.
488 Western blot quantifications were performed using Image Lab software (BioRad), and LC3-II levels
489 were quantified after normalization by the strain free (total amounts of proteins/lane).

490 **Small interfering RNA transfection.** For siRNA transfection, cells were seeded at confluence of
491 $0{,}1 \times 10^6$ cells/mL in 24-well plate (TPP) the day before transfection. In each well, transfection was
492 performed using 4,5 µL of Lipofectamine siRNA Max reagent (ThermoFisher) in 650 µL of OptiMEM
493 media (Gibco) and according to the manufacturer's instructions. The final concentration of commercial
494 predesigned siRNA targeting *p62* and *nrf2* (FlexiTube, Qiagen) was 80 nM and the corresponding
495 scramble siRNA (all start negative, Qiagen) was performed as control. The siRNA preparations in
496 lipofectamine were incubated at room temperature for 25 min before delicate transfection of the cells.
497 After 12 hours, 350 µL of complete RPMI was added on the cells. The infection was performed 24 hours
498 post-transfection in complete RPMI and the reduction in p62 and NRF2 levels was checked by HCS
499 microscopy.

500 **ELISA and Griess reaction**. Fresh cell culture supernatants were used 24 h post-infection for dosage
501 of nitric oxide (NO) by the Griess reaction. On the other hand, cytokine dosage was performed on frozen
502 supernatants by ELISA using DuoSet kits (R&D Systems), according to the manufacturer's instructions.

503 **Viability and LDH release assays**. LDH release was measured using the CyQuant LDH Cytotoxicity
504 Assay kit (fresh supernatant) (Invitrogen), according to the manufacturers' instructions. On the other
505 hand, viability was measured using MTT assay: after infection, cells were incubated for 2 h in 1 mg/mL
506 MTT solution (Sigma) in complete RPMI. MTT crystals were then dissolved in HCl 1 M, isopropanol
507 (1:24) and absorbance was read at 595 nm.

508 **RT-qPCR.** RNAs were extracted from frozen cells using RNeasy Mini Kit (Qiagen) according to the
509 manufacturer's instructions. cDNAs were then obtained by retro-transcription (RT) using SuperScript II
510 RT (Invitrogen). The equivalent of 20ng of cDNA were used for RT-qPCR with specific primers and
511 probes (**Table 2**). qPCR was performed using Taqman Universal MasterMix (Applied Biosystems) on
512 a StepOne Plus Real Time PCR System (Applied Biosystems) with the standard protocol. Fold changes
513 were calculated with the $2^{-\Delta\Delta Ct}$ method, using hypoxanthine guanine phosphoribosyl transferase (HPRT)
514 as internal control.

516 **Table 2.** Primers and probe list for RT-qPCR analyses

Target	Forward primer sequence	Reverse primer sequence	Probe sequence
p62	5'-ATGTGGAACATGGAGGGAAGAG-3'	5'-TTCTGTGCCTGTGCTGGAACT-3'	5'-CCGCCTGACACCCACTACCCCA-3'
lc3	5'-GCCCCACCCCTGAAAGG-3'	5'-TGCAGAGGAAATGACCACAGAT-3'	5'-TGGCTCCCCTTGTCCTGACTCGG-3'
iNOS	5'-CATGACTGCTAATGTCAGAG-3'	5'-TCCTAGTCCATCCGGATAAA-3'	5'-GAAATCTGAGTTTGGCCTGAGG-3'
tnf	5'-CATCTTCTCAAAATTCGAGTGACAA-3'	5'-TGGGAGTAGACAAGGTACAACCC-3'	5'-CACGTCGTAGCAAACCACCAAGTGGA-3'
il6	5'-CTCCAGCTTATCTGTTAGGA-3'	5'-CTTCAACCAAGAGGTAAAAGA-3'	5'-AAATTGGGGTAGGAAGGACTATTTTATG-3'
il10	5'-GGCGCTGTCATCGATTTCTC-3'	5'-GACACCTTGGTCTTGGAGCTTATTAA-3'	5'-AAAATAAGAGCAAGGCAGTGGAGCAGGTG-3'
hprt	5'-CTGGTGAAAAGGACCTCTCGA-3'	5'-TGCCCTTGACTATAATGAGTACTTCA-3'	5'-TGTTGGATACAGGCCAGACTTTGTTGGAT-3'
cat	Pre-designed: Mm00437992_m1 (ThermoFisher)		
gsr	Pre-designed: Mm01197925_m1 (ThermoFisher)		
hprt	Pre-designed: Mm03024075_m1 (ThermoFisher)		

517

518 **Statistical analyses.** All statistical analyses were performed using Student's *t*-test with
519 corresponding p values: * for $p < 0.05$; ** for $p < 0.01$ and *** for $p < 0.001$.

520 ACKNOWLEDGMENTS

521 We acknowledge Nathalie Aulner and Anne Danckaert (Institut Pasteur) as well as the Photonic
522 BioImaging Unit of Technology and Service, a member of the France-BioImaging infrastructure, for
523 support in conducting this study.

524 FUNDING

525 This work was funded by Institut Pasteur grant PTR2017-66 to CW and by Agence Nationale de la
526 Recherche (ANR) grant ANR-10-LABX-62-IBEID to IGB. DB was funded by Université Paris Cité
527 (formerly Université Paris Diderot) through Doctoral school FIRE (ED FIRE474). IS has been part of
528 the Pasteur-Paris University (PPU) International PhD program. This program has received funding from
529 the Institut Carnot Pasteur Microbes & Santé, and the European Union's Horizon 2020 research and
530 innovation program under the Marie Sklodowska-Curie grant agreement no. 665807. IS has additionally
531 benefited from a scholarship "Fin de thèse de science" number FDT201805005258 granted by
532 "Fondation pour la recherche médicale (FRM)". France-BioImaging infrastructure network is supported
533 by the French National Research Agency (ANR-10–INSB–04, Investments for the future). The use of
534 the Opera Phenix system in the PBI core facility has been made possible by the kind financial support
535 of the Institut Pasteur (Paris) and the Région Ile-de-France (program DIM1Health). The authors declare
536 no conflict of interest.

538 **AUTHORS CONTRIBUTIONS**

539 Conception, administration, and supervision of the project: CW.
540 Investigation: DB, IS, and CW.
541 Methodology: IS, DB and PE.
542 Data analysis: DB, IS, PE and CW.
543 Visualization: DB.
544 Validation: IS, DB and CW.
545 Resources: FVP.
546 Funding acquisition: CW and IGB.
547 DB and IS wrote the original draft, under CW's supervision.
548 All authors contributed to the review of the manuscript and approved it for submission.

549

550 **REFERENCES**

551 1. Costa F, Hagan JE, Calcagno J, Kane M, Torgerson P, Martinez-Silveira MS, et al. Global Morbidity and
552 Mortality of Leptospirosis: A Systematic Review. PLoS Negl Trop Dis. 2015;9(9):e0003898. Epub
553 20150917. doi: 10.1371/journal.pntd.0003898. PubMed PMID: 26379143; PubMed Central PMCID:
554 PMCPMC4574773.

555 2. Adler B. History of leptospirosis and leptospira. Curr Top Microbiol Immunol. 2015;387:1-9. doi:
556 10.1007/978-3-662-45059-8_1. PubMed PMID: 25388129.

557 3. Ko AI, Goarant C, Picardeau M. Leptospira: the dawn of the molecular genetics era for an emerging zoonotic
558 pathogen. Nat Rev Microbiol. 2009;7(10):736-47. doi: 10.1038/nrmicro2208. PubMed PMID: 19756012;
559 PubMed Central PMCID: PMCPMC3384523.

560 4. Ratet G, Veyrier FJ, Fanton d'Andon M, Kammerscheit X, Nicola MA, Picardeau M, et al. Live imaging of
561 bioluminescent leptospira interrogans in mice reveals renal colonization as a stealth escape from the blood
562 defenses and antibiotics. PLoS Negl Trop Dis. 2014;8(12):e3359. Epub 20141204. doi:
563 10.1371/journal.pntd.0003359. PubMed PMID: 25474719; PubMed Central PMCID: PMCPMC4256284.

564 5. Werts C, Tapping RI, Mathison JC, Chuang TH, Kravchenko V, Saint Girons I, et al. Leptospiral
565 lipopolysaccharide activates cells through a TLR2-dependent mechanism. Nat Immunol. 2001;2(4):346-52.
566 doi: 10.1038/86354. PubMed PMID: 11276206.

567 6. Hsu SH, Hung CC, Chang MY, Ko YC, Yang HY, Hsu HH, et al. Active Components of Leptospira Outer
568 Membrane Protein LipL32 to Toll-Like Receptor 2. Sci Rep. 2017;7(1):8363. Epub 20170821. doi:
569 10.1038/s41598-017-08743-y. PubMed PMID: 28827637; PubMed Central PMCID: PMCPMC5566480.

570 7. Ratet G, Santecchia I, Fanton d'Andon M, Vernel-Pauillac F, Wheeler R, Lenormand P, et al. LipL21
571 lipoprotein binding to peptidoglycan enables Leptospira interrogans to escape NOD1 and NOD2 recognition.
572 PLoS Pathog. 2017;13(12):e1006725. Epub 20171206. doi: 10.1371/journal.ppat.1006725. PubMed PMID:
573 29211798; PubMed Central PMCID: PMCPMC5764436.

574 8. Holzapfel M, Bonhomme D, Cagliero J, Vernel-Pauillac F, Fanton d'Andon M, Bortolussi S, et al. Escape of
575 TLR5 Recognition by Leptospira spp.: A Rationale for Atypical Endoflagella. Front Immunol. 2020;11:2007.
576 Epub 20200811. doi: 10.3389/fimmu.2020.02007. PubMed PMID: 32849665; PubMed Central PMCID:
577 PMCPMC7431986.

578 9. Murray GL, Srikram A, Henry R, Hartskeerl RA, Sermswan RW, Adler B. Mutations affecting Leptospira
579 interrogans lipopolysaccharide attenuate virulence. Mol Microbiol. 2010;78(3):701-9. Epub 20100914. doi:
580 10.1111/j.1365-2958.2010.07360.x. PubMed PMID: 20807198.

581 10. Que-Gewirth NL, Ribeiro AA, Kalb SR, Cotter RJ, Bulach DM, Adler B, et al. A methylated phosphate
582 group and four amide-linked acyl chains in leptospira interrogans lipid A. The membrane anchor of an
583 unusual lipopolysaccharide that activates TLR2. J Biol Chem. 2004;279(24):25420-9. Epub 20040324. doi:
584 10.1074/jbc.M400598200. PubMed PMID: 15044492; PubMed Central PMCID: PMCPMC2556802.

585 11. Bonhomme D, Santecchia I, Vernel-Pauillac F, Caroff M, Germon P, Murray G, et al. Leptospiral LPS
586 escapes mouse TLR4 internalization and TRIFassociated antimicrobial responses through O antigen and
587 associated lipoproteins. PLoS Pathog. 2020;16(8):e1008639. Epub 20200813. doi:
588 10.1371/journal.ppat.1008639. PubMed PMID: 32790743; PubMed Central PMCID: PMCPMC7447051.

589 12. Lacroix-Lamande S, d'Andon MF, Michel E, Ratet G, Philpott DJ, Girardin SE, et al. Downregulation of the
590 Na/K-ATPase pump by leptospiral glycolipoprotein activates the NLRP3 inflammasome. J Immunol.
591 2012;188(6):2805-14. Epub 20120208. doi: 10.4049/jimmunol.1101987. PubMed PMID: 22323544.

592 13. Santecchia I, Bonhomme D, Papadopoulos S, Escoll P, Giraud-Gatineau A, Moya-Nilges M, et al. Alive
593 Pathogenic and Saprophytic Leptospires Enter and Exit Human and Mouse Macrophages With No
594 Intracellular Replication. Front Cell Infect Microbiol 2022;12:936931. doi: doi: 10.3389/fcimb.2022.936931.

595 14. Sorbara MT, Ellison LK, Ramjeet M, Travassos LH, Jones NL, Girardin SE, et al. The protein ATG16L1
596 suppresses inflammatory cytokines induced by the intracellular sensors Nod1 and Nod2 in an autophagy-
597 independent manner. Immunity. 2013;39(5):858-73. doi: 10.1016/j.immuni.2013.10.013. PubMed PMID:
598 24238340.

599 15. Wang Z, Li C. Xenophagy in innate immunity: A battle between host and pathogen. Dev Comp Immunol.
600 2020;109:103693. Epub 20200331. doi: 10.1016/j.dci.2020.103693. PubMed PMID: 32243873.

601 16. Travassos LH, Carneiro LA, Girardin S, Philpott DJ. Nod proteins link bacterial sensing and autophagy.
602 Autophagy. 2010;6(3):409-11. Epub 20100426. doi: 10.4161/auto.6.3.11305. PubMed PMID: 20200479.

603 17. Birmingham CL, Smith AC, Bakowski MA, Yoshimori T, Brumell JH. Autophagy controls Salmonella
604 infection in response to damage to the Salmonella-containing vacuole. J Biol Chem. 2006;281(16):11374-
605 83. Epub 20060222. doi: 10.1074/jbc.M509157200. PubMed PMID: 16495224.

606 18. Gutierrez MG, Master SS, Singh SB, Taylor GA, Colombo MI, Deretic V. Autophagy is a defense
607 mechanism inhibiting BCG and Mycobacterium tuberculosis survival in infected macrophages. Cell.
608 2004;119(6):753-66. doi: 10.1016/j.cell.2004.11.038. PubMed PMID: 15607973.

609 19. He C, Klionsky DJ. Regulation mechanisms and signaling pathways of autophagy. Annu Rev Genet.
610 2009;43:67-93. doi: 10.1146/annurev-genet-102808-114910. PubMed PMID: 19653858; PubMed Central
611 PMCID: PMCPMC2831538.

612 20. Mizushima N, Kuma A, Kobayashi Y, Yamamoto A, Matsubae M, Takao T, et al. Mouse Apg16L, a novel
613 WD-repeat protein, targets to the autophagic isolation membrane with the Apg12-Apg5 conjugate. J Cell Sci.
614 2003;116(Pt 9):1679-88. doi: 10.1242/jcs.00381. PubMed PMID: 12665549.

615 21. Tanida I, Ueno T, Kominami E. LC3 conjugation system in mammalian autophagy. Int J Biochem Cell Biol.
616 2004;36(12):2503-18. doi: 10.1016/j.biocel.2004.05.009. PubMed PMID: 15325588; PubMed Central
617 PMCID: PMCPMC7129593.

618 22. Hanada T, Noda NN, Satomi Y, Ichimura Y, Fujioka Y, Takao T, et al. The Atg12-Atg5 conjugate has a
619 novel E3-like activity for protein lipidation in autophagy. J Biol Chem. 2007;282(52):37298-302. Epub
620 20071106. doi: 10.1074/jbc.C700195200. PubMed PMID: 17986448.

621 23. Kabeya Y, Mizushima N, Ueno T, Yamamoto A, Kirisako T, Noda T, et al. LC3, a mammalian homologue
622 of yeast Apg8p, is localized in autophagosome membranes after processing. EMBO J. 2000;19(21):5720-8.
623 doi: 10.1093/emboj/19.21.5720. PubMed PMID: 11060023; PubMed Central PMCID: PMCPMC305793.

624 24. Klionsky DJ, Abdel-Aziz AK, Abdelfatah S, Abdellatif M, Abdoli A, Abel S, et al. Guidelines for the use
625 and interpretation of assays for monitoring autophagy (4th edition)(1). Autophagy. 2021;17(1):1-382. Epub
626 20210208. doi: 10.1080/15548627.2020.1797280. PubMed PMID: 33634751; PubMed Central PMCID:
627 PMCPMC7996087.

628 25. Xu Y, Jagannath C, Liu XD, Sharafkhaneh A, Kolodziejska KE, Eissa NT. Toll-like receptor 4 is a sensor
629 for autophagy associated with innate immunity. Immunity. 2007;27(1):135-44. Epub 20070719. doi:
630 10.1016/j.immuni.2007.05.022. PubMed PMID: 17658277; PubMed Central PMCID: PMCPMC2680670.

631 26. Travassos LH, Carneiro LA, Ramjeet M, Hussey S, Kim YG, Magalhaes JG, et al. Nod1 and Nod2 direct
632 autophagy by recruiting ATG16L1 to the plasma membrane at the site of bacterial entry. Nat Immunol.
633 2010;11(1):55-62. Epub 20091108. doi: 10.1038/ni.1823. PubMed PMID: 19898471.

634 27. Birmingham CL, Canadien V, Gouin E, Troy EB, Yoshimori T, Cossart P, et al. Listeria monocytogenes
635 evades killing by autophagy during colonization of host cells. Autophagy. 2007;3(5):442-51. Epub 20070518.
636 doi: 10.4161/auto.4450. PubMed PMID: 17568179.

637 28. Case ED, Chong A, Wehrly TD, Hansen B, Child R, Hwang S, et al. The Francisella O-antigen mediates
638 survival in the macrophage cytosol via autophagy avoidance. Cell Microbiol. 2014;16(6):862-77. Epub
639 20131216. doi: 10.1111/cmi.12246. PubMed PMID: 24286610; PubMed Central PMCID:
640 PMCPMC4028363.

641 29. Kreibich S, Emmenlauer M, Fredlund J, Ramo P, Munz C, Dehio C, et al. Autophagy Proteins Promote
642 Repair of Endosomal Membranes Damaged by the Salmonella Type Three Secretion System 1. Cell Host
643 Microbe. 2015;18(5):527-37. doi: 10.1016/j.chom.2015.10.015. PubMed PMID: 26567507.

644 30. Chen Z, Wang T, Liu Z, Zhang G, Wang J, Feng S, et al. Inhibition of Autophagy by MiR-30A Induced by
645 Mycobacteria tuberculosis as a Possible Mechanism of Immune Escape in Human Macrophages. Jpn J Infect
646 Dis. 2015;68(5):420-4. Epub 20150410. doi: 10.7883/yoken.JJID.2014.466. PubMed PMID: 25866116.

647 31. Choy A, Dancourt J, Mugo B, O'Connor TJ, Isberg RR, Melia TJ, et al. The Legionella effector RavZ inhibits
648 host autophagy through irreversible Atg8 deconjugation. Science. 2012;338(6110):1072-6. Epub 20121025.
649 doi: 10.1126/science.1227026. PubMed PMID: 23112293; PubMed Central PMCID: PMCPMC3682818.

650 32. Ogawa M, Yoshimori T, Suzuki T, Sagara H, Mizushima N, Sasakawa C. Escape of intracellular Shigella
651 from autophagy. Science. 2005;307(5710):727-31. Epub 20041202. doi: 10.1126/science.1106036. PubMed
652 PMID: 15576571.

653 33. Manzanillo PS, Ayres JS, Watson RO, Collins AC, Souza G, Rae CS, et al. The ubiquitin ligase parkin
654 mediates resistance to intracellular pathogens. Nature. 2013;501(7468):512-6. Epub 20130904. doi:
655 10.1038/nature12566. PubMed PMID: 24005326; PubMed Central PMCID: PMCPMC3886920.

656 34. Mostowy S, Sancho-Shimizu V, Hamon MA, Simeone R, Brosch R, Johansen T, et al. p62 and NDP52
657 proteins target intracytosolic Shigella and Listeria to different autophagy pathways. J Biol Chem.
658 2011;286(30):26987-95. Epub 20110606. doi: 10.1074/jbc.M111.223610. PubMed PMID: 21646350;
659 PubMed Central PMCID: PMCPMC3143657.

660 35. Watson RO, Bell SL, MacDuff DA, Kimmey JM, Diner EJ, Olivas J, et al. The Cytosolic Sensor cGAS
661 Detects Mycobacterium tuberculosis DNA to Induce Type I Interferons and Activate Autophagy. Cell Host
662 Microbe. 2015;17(6):811-9. Epub 20150602. doi: 10.1016/j.chom.2015.05.004. PubMed PMID: 26048136;
663 PubMed Central PMCID: PMCPMC4466081.

664 36. Zheng YT, Shahnazari S, Brech A, Lamark T, Johansen T, Brumell JH. The adaptor protein p62/SQSTM1
665 targets invading bacteria to the autophagy pathway. J Immunol. 2009;183(9):5909-16. Epub 20091007. doi:
666 10.4049/jimmunol.0900441. PubMed PMID: 19812211.

667 37. Wlodarska M, Thaiss CA, Nowarski R, Henao-Mejia J, Zhang JP, Brown EM, et al. NLRP6 inflammasome
668 orchestrates the colonic host-microbial interface by regulating goblet cell mucus secretion. Cell.
669 2014;156(5):1045-59. doi: 10.1016/j.cell.2014.01.026. PubMed PMID: 24581500; PubMed Central PMCID:
670 PMCPMC4017640.

671 38. Jounai N, Kobiyama K, Shiina M, Ogata K, Ishii KJ, Takeshita F. NLRP4 negatively regulates autophagic
672 processes through an association with beclin1. J Immunol. 2011;186(3):1646-55. Epub 20110105. doi:
673 10.4049/jimmunol.1001654. PubMed PMID: 21209283.

674 39. Deng Q, Wang Y, Zhang Y, Li M, Li D, Huang X, et al. Pseudomonas aeruginosa Triggers Macrophage
675 Autophagy To Escape Intracellular Killing by Activation of the NLRP3 Inflammasome. Infect Immun.
676 2016;84(1):56-66. Epub 20151014. doi: 10.1128/IAI.00945-15. PubMed PMID: 26467446; PubMed Central
677 PMCID: PMCPMC4694000.

678 40. Lai M, Yao H, Shah SZA, Wu W, Wang D, Zhao Y, et al. The NLRP3-Caspase 1 Inflammasome Negatively
679 Regulates Autophagy via TLR4-TRIF in Prion Peptide-Infected Microglia. Front Aging Neurosci.
680 2018;10:116. Epub 20180418. doi: 10.3389/fnagi.2018.00116. PubMed PMID: 29720937; PubMed Central
681 PMCID: PMCPMC5915529.

682 41. Jain A, Lamark T, Sjottem E, Larsen KB, Awuh JA, Overvatn A, et al. p62/SQSTM1 is a target gene for
683 transcription factor NRF2 and creates a positive feedback loop by inducing antioxidant response element-
684 driven gene transcription. J Biol Chem. 2010;285(29):22576-91. Epub 20100507. doi:
685 10.1074/jbc.M110.118976. PubMed PMID: 20452972; PubMed Central PMCID: PMCPMC2903417.

686 42. Komatsu M, Kurokawa H, Waguri S, Taguchi K, Kobayashi A, Ichimura Y, et al. The selective autophagy
687 substrate p62 activates the stress responsive transcription factor Nrf2 through inactivation of Keap1. Nat Cell
688 Biol. 2010;12(3):213-23. Epub 20100221. doi: 10.1038/ncb2021. PubMed PMID: 20173742.

43. Lau A, Wang XJ, Zhao F, Villeneuve NF, Wu T, Jiang T, et al. A noncanonical mechanism of Nrf2 activation by autophagy deficiency: direct interaction between Keap1 and p62. Mol Cell Biol. 2010;30(13):3275-85. Epub 20100426. doi: 10.1128/MCB.00248-10. PubMed PMID: 20421418; PubMed Central PMCID: PMCPMC2897585.

44. Kong X, Thimmulappa R, Craciun F, Harvey C, Singh A, Kombairaju P, et al. Enhancing Nrf2 pathway by disruption of Keap1 in myeloid leukocytes protects against sepsis. Am J Respir Crit Care Med. 2011;184(8):928-38. Epub 20110728. doi: 10.1164/rccm.201102-0271OC. PubMed PMID: 21799073; PubMed Central PMCID: PMCPMC3208662.

45. Kobayashi EH, Suzuki T, Funayama R, Nagashima T, Hayashi M, Sekine H, et al. Nrf2 suppresses macrophage inflammatory response by blocking proinflammatory cytokine transcription. Nat Commun. 2016;7:11624. Epub 20160523. doi: 10.1038/ncomms11624. PubMed PMID: 27211851; PubMed Central PMCID: PMCPMC4879264.

46. Abby SS, Cury J, Guglielmini J, Neron B, Touchon M, Rocha EP. Identification of protein secretion systems in bacterial genomes. Sci Rep. 2016;6:23080. Epub 20160316. doi: 10.1038/srep23080. PubMed PMID: 26979785; PubMed Central PMCID: PMCPMC4793230.

47. Nahori MA, Fournie-Amazouz E, Que-Gewirth NS, Balloy V, Chignard M, Raetz CR, et al. Differential TLR recognition of leptospiral lipid A and lipopolysaccharide in murine and human cells. J Immunol. 2005;175(9):6022-31. doi: 10.4049/jimmunol.175.9.6022. PubMed PMID: 16237097.

48. Bonhomme D, Hernandez-Trejo V, Papadopoulos S, Pigache R, Fanton d'Andon M, Outlia A, et al. *Leptospira interrogans* prevents macrophage cell death and pyroptotic IL1ß releasethrough atypical lipopolysaccharide. BioRXiv. doi: 10.1101/2022.07.25.501344.

49. Terawaki S, Camosseto V, Prete F, Wenger T, Papadopoulos A, Rondeau C, et al. RUN and FYVE domain-containing protein 4 enhances autophagy and lysosome tethering in response to Interleukin-4. J Cell Biol. 2015;210(7):1133-52. doi: 10.1083/jcb.201501059. PubMed PMID: 26416964; PubMed Central PMCID: PMCPMC4586740.

50. Ye X, Zhu M, Che X, Wang H, Liang XJ, Wu C, et al. Lipopolysaccharide induces neuroinflammation in microglia by activating the MTOR pathway and downregulating Vps34 to inhibit autophagosome formation. J Neuroinflammation. 2020;17(1):18. Epub 20200111. doi: 10.1186/s12974-019-1644-8. PubMed PMID: 31926553; PubMed Central PMCID: PMCPMC6954631.

51. Yin S, Cao W. Toll-Like Receptor Signaling Induces Nrf2 Pathway Activation through p62-Triggered Keap1 Degradation. Mol Cell Biol. 2015;35(15):2673-83. Epub 20150526. doi: 10.1128/MCB.00105-15. PubMed PMID: 26012548; PubMed Central PMCID: PMCPMC4524114.

52. Jiang T, Harder B, Rojo de la Vega M, Wong PK, Chapman E, Zhang DD. p62 links autophagy and Nrf2 signaling. Free Radic Biol Med. 2015;88(Pt B):199-204. Epub 20150624. doi: 10.1016/j.freeradbiomed.2015.06.014. PubMed PMID: 26117325; PubMed Central PMCID: PMCPMC4628872.

53. Gilardini Montani MS, Santarelli R, Granato M, Gonnella R, Torrisi MR, Faggioni A, et al. EBV reduces autophagy, intracellular ROS and mitochondria to impair monocyte survival and differentiation. Autophagy. 2019;15(4):652-67. Epub 20181023. doi: 10.1080/15548627.2018.1536530. PubMed PMID: 30324853; PubMed Central PMCID: PMCPMC6526866.

54. Bichiou H, Rabhi S, Ben Hamda C, Bouabid C, Belghith M, Piquemal D, et al. Leishmania Parasites Differently Regulate Antioxidant Genes in Macrophages Derived From Resistant and Susceptible Mice. Front Cell Infect Microbiol. 2021;11:748738. Epub 20211015. doi: 10.3389/fcimb.2021.748738. PubMed PMID: 34722338; PubMed Central PMCID: PMCPMC8554229.

55. Zavala-Alvarado C, Sismeiro O, Legendre R, Varet H, Bussotti G, Bayram J, et al. The transcriptional response of pathogenic Leptospira to peroxide reveals new defenses against infection-related oxidative stress. PLoS Pathog. 2020;16(10):e1008904. Epub 20201006. doi: 10.1371/journal.ppat.1008904. PubMed PMID: 33021995; PubMed Central PMCID: PMCPMC7567364.

56. Vivarini AC, Calegari-Silva TC, Saliba AM, Boaventura VS, Franca-Costa J, Khouri R, et al. Systems Approach Reveals Nuclear Factor Erythroid 2-Related Factor 2/Protein Kinase R Crosstalk in Human Cutaneous Leishmaniasis. Front Immunol. 2017;8:1127. Epub 20170915. doi: 10.3389/fimmu.2017.01127. PubMed PMID: 28959260; PubMed Central PMCID: PMCPMC5605755.

741 57. Macoch M, Morzadec C, Genard R, Pallardy M, Kerdine-Romer S, Fardel O, et al. Nrf2-dependent repression
742 of interleukin-12 expression in human dendritic cells exposed to inorganic arsenic. Free Radic Biol Med.
743 2015;88(Pt B):381-90. Epub 20150211. doi: 10.1016/j.freeradbiomed.2015.02.003. PubMed PMID:
744 25680285.

745 58. Helou DG, Braham S, De Chaisemartin L, Granger V, Damien MH, Pallardy M, et al. Nrf2 downregulates
746 zymosan-induced neutrophil activation and modulates migration. PLoS One. 2019;14(8):e0216465. Epub
747 20190816. doi: 10.1371/journal.pone.0216465. PubMed PMID: 31419224; PubMed Central PMCID:
748 PMCPMC6697320.

749 59. Fanton d'Andon M, Quellard N, Fernandez B, Ratet G, Lacroix-Lamande S, Vandewalle A, et al. Leptospira
750 Interrogans induces fibrosis in the mouse kidney through Inos-dependent, TLR- and NLR-independent
751 signaling pathways. PLoS Negl Trop Dis. 2014;8(1):e2664. Epub 20140130. doi:
752 10.1371/journal.pntd.0002664. PubMed PMID: 24498450; PubMed Central PMCID: PMCPMC3907306.

753 60. Raffray L, Giry C, Vandroux D, Kuli B, Randrianjohany A, Pequin AM, et al. Major Neutrophilia Observed
754 in Acute Phase of Human Leptospirosis Is Not Associated with Increased Expression of Granulocyte Cell
755 Activation Markers. PLoS One. 2016;11(11):e0165716. Epub 20161101. doi: 10.1371/journal.pone.0165716.
756 PubMed PMID: 27802348; PubMed Central PMCID: PMCPMC5089758.

757 61. Olagnier D, Brandtoft AM, Gunderstofte C, Villadsen NL, Krapp C, Thielke AL, et al. Nrf2 negatively
758 regulates STING indicating a link between antiviral sensing and metabolic reprogramming. Nat Commun.
759 2018;9(1):3506. Epub 20180829. doi: 10.1038/s41467-018-05861-7. PubMed PMID: 30158636; PubMed
760 Central PMCID: PMCPMC6115435.

761 62. Werts C, le Bourhis L, Liu J, Magalhaes JG, Carneiro LA, Fritz JH, et al. Nod1 and Nod2 induce
762 CCL5/RANTES through the NF-kappaB pathway. Eur J Immunol. 2007;37(9):2499-508. doi:
763 10.1002/eji.200737069. PubMed PMID: 17705131.

764 63. Santecchia I, Vernel-Pauillac F, Rasid O, Quintin J, Gomes-Solecki M, Boneca IG, et al. Innate immune
765 memory through TLR2 and NOD2 contributes to the control of Leptospira interrogans infection. PLoS
766 Pathog. 2019;15(5):e1007811. Epub 20190520. doi: 10.1371/journal.ppat.1007811. PubMed PMID:
767 31107928; PubMed Central PMCID: PMCPMC6544334.

768 64. Bonhomme D, Werts C. Purification of LPS from Leptospira. Methods Mol Biol. 2020;2134:53-65. doi:
769 10.1007/978-1-0716-0459-5_6. PubMed PMID: 32632859.

770

772 **FIGURES LEGENDS**

773 **Figure 1. *L. interrogans* reduces the quantity of autophagosomes in macrophages**

774 **A)** WB of LC3 in C57/BL6 mouse peritoneal cells 4 h post-intraperitoneal injection of PBS, 5 x 10^7
775 *L. interrogans* serovar Manilae strain MFLum1 (*L.i*), 30 µg of muropeptides (murP) (MDP+FK156) or
776 30 µg of rapamycin (Rap). **B)** WB of LC3 in BMDMs 24 h post-infection with either live or heat-killed
777 (HK) *L. interrogans* serovar Manilae strain MFLum1 at MOI 100, or stimulation with 500 nM
778 rapamycin. **C)** WB of LC3 in BMDMs 24 h post-infection with *L. interrogans* serovar Manilae strain
779 MFLum1 at MOI 100, with or without bafilomycin A1 (BafA1) addition 4 h before cell collection. **D)**
780 WB analyses and quantifications of LC3 in BMDMs 1 h, 4 h and 24 h post-infection with either live or
781 HK *L. interrogans* serovar Manilae strain MFLum1 at MOI 100. Quantifications represent the ratio of
782 LC3-II in stimulated cells over non-stimulated cells, and after stain free normalization. Each dot
783 corresponds to the quantification of a blot from an independent experiment (*n* from 3 to 6). **E)** RT-qPCR
784 analyses of LC3 mRNA levels in BMDMs 24 h post-infection with MOI 100 of *L. interrogans* serovar
785 Manilae strain L495. Bars correspond to mean +/- SD of technical replicates (*n*=4). **F-G)** High Content
786 (HC) confocal microscopy images and quantifications of RAW-mLC3-DiFluo cells 4 h post-infection
787 with *L. interrogans* serovar Manilae strain MFLum1 at MOI 100, with or without bafilomycin A1
788 (BafA1) addition 2 h before cell fixation. Bars correspond to mean +/- SD of technical replicates (*n*=4).
789 **A-E)** Data presented are representative of at least 3 independent experiments.

790 **Figure 2. *L. interrogans* induces specific accumulation of p62 adaptor in puncta-like structures**

791 **A)** WB of p62 in BMDMs 1 h, 4 h and 24 h post-infection with *L. interrogans* serovar Manilae strain
792 MFLum1. **B)** WB of p62 in BMDMs 24 h post-infection with *L. interrogans* serovar Manilae strain
793 MFLum1, serovar Copenhageni strain Fiocruz L1-130, serovar Icterohaemorrhagiae strain Verdun, and
794 *L. biflexa* serovar Patoc strain Patoc I. **C)** RT-qPCR analyses of p62 mRNA levels in BMDMs 24 h
795 post-infection with *L. interrogans* serovar Manilae strain L495. Bars correspond to mean +/- SD of
796 technical replicates (*n*=4). **D)** Epifluorescence analyses of p62 in BMDMs 4 h post-infection with
797 *L. interrogans* serovar Manilae strain MFLum1. **E)** High Content (HC) confocal microscopy analyses
798 of the number of p62 puncta *per* cell and the percentage of p62 positive cells 1 h, 4 h and 24 h
799 post-infection of RAW264.7 cells with *L. interrogans* serovar Manilae strain L495. **F)** HC single cell
800 microscopy analysis of the number of p62 puncta *per* cell 24 h post-infection of RAW264.7 cells with
801 *L. interrogans* serovar Manilae strain L495. **A-F)** Data presented are representative of at least 3
802 independent experiments.

803 **Figure 3. Autophagy modulation is mediated by TLR2/TLR4**

804 **A)** WB of LC3 and p62 in WT and TLR2/4 dko BMDMs 24 h post-infection with *L. interrogans* serovar
805 Manilae strain MFLum1 at MOI 100, or upon starvation induction by incubation in EBSS medium.
806 **B)** WB of p62 in WT and MyD88/TRIF dko BMDMs 24 h post-infection with *L. interrogans* serovar
807 Manilae strain MFLum1. **C)** RT-qPCR analyses of p62 mRNA levels in WT and TLR2/4 dko BMDMs
808 24 h post-infection with *L. interrogans* serovar Manilae strain L495 at MOI 100. Bars correspond to
809 mean of independent experiments (*n*=3). **D)** High Content (HC) single cell microscopy analysis of the
810 number of p62 puncta *per* cell 24 h post-infection of WT, TLR2/TLR4 dko and MyD88/TRIF dko
811 BMDMs with *L. interrogans* serovar Manilae strain L495, serovar Copenhageni strain Fiocruz L1-130

812 and serovar Icterohaemorrhagiae strain Verdun. **A-D)** Data presented are representative of at least 2
813 independent experiments.

814 **Figure 4. p62 accumulation is mediated by the leptospiral LPS**

815 **A)** WB of p62 in BMDMs 1 h, 4 h and 24 h post-stimulation with heat-killed (56°C, 30 min)
816 *L. interrogans* serovar Manilae strain MFLum1 at MOI 100 or 24 h post-stimulation with 1 µg/mL of
817 the corresponding purified leptospiral LPS. **B)** High Content (HC) confocal microscopy analyses of the
818 number of p62 puncta *per* cell and the percentage of p62 positive cells 1 h, 4 h and 24 h post-stimulation
819 of RAW264.7 cells with MOI 100 of either live or heat-killed (56°C, 30 min) *L. interrogans* serovar
820 Manilae strain L495 or stimulation with 1 µg/mL of the corresponding purified leptospiral LPS. **C)** HC
821 single cell microscopy analysis of the number of p62 puncta *per* cell 24 h post-infection of RAW264.7
822 cells with MOI 100 of either live or heat-killed (56°C, 30 min) *L. interrogans* serovar Manilae strain
823 L495 or stimulation with 1 µg/mL of the corresponding purified leptospiral LPS. **A-C)** Data presented
824 are representative of at least 3 independent experiments.

825 **Figure 5. Leptospiral LPS also triggers translocation of NRF2 transcription factor**

826 **A)** Confocal microscopy analyses of NRF2 in BMDMs 4 h post-infection with *L. interrogans* serovar
827 Manilae strain L495 at MOI 100. **B)** High Content (HC) single cell microscopy analysis of the levels of
828 NRF2 intensity in the nucleus and 4 h post-infection of RAW264.7 cells with *L. interrogans* serovar
829 Manilae strain L495, serovar Copenhageni strain Fiocruz L1-130 or serovar Icterohaemorrhagiae strain
830 Verdun, at MOI 100. Fluorescence is expressed in arbitrary units (AU), dashed lines correspond to
831 median. **C)** HC analysis of the number of cells with NRF2 intensity ratio [nucleus/cytoplasm] > 1.4 4 h
832 post-infection of RAW264.7 cells with *L. interrogans* serovar Manilae strain L495, serovar
833 Copenhageni strain Fiocruz L1-130 or serovar Icterohaemorrhagiae strain Verdun, at MOI 100. **D)** HC
834 single cell microscopy analysis of the levels of NRF2 intensity in the nucleus 4 h post-infection of
835 RAW264.7 cells with MOI 100 of either live or heat-killed (56°C, 30 min) *L. interrogans* serovar
836 Manilae strain L495 or stimulation with 1 µg/mL of the corresponding purified leptospiral LPS.
837 Fluorescence is expressed in arbitrary units (AU), dashed lines correspond to median. **E)** HC analysis
838 of the number of cells with NRF2 intensity ratio [nucleus/cytoplasm] > 1.4 4 h post-infection of
839 RAW264.7 cells with MOI 100 of either live or heat-killed (56°C, 30 min) *L. interrogans* serovar
840 Manilae strain L495 or stimulation with 1 µg/mL of the corresponding purified leptospiral LPS.
841 **A-E)** Data presented are representative of at least 2 independent experiments.

842 **Figure 6. p62 and NRF2 constitute a retro-activation loop upon infection with *L. interrogans***

843 **A)** High Content (HC) single cell microscopy analysis of NRF2 intensity ratio [nucleus/cytoplasm] in
844 BMDMs transfected with scramble (scrbl) or p62 siRNA and infected for 4 h with *L. interrogans* serovar
845 Manilae strain L495 at MOI 100. **B)** Corresponding controls are microscopy analyses and quantification
846 of p62 intensity in the same transfection and infection conditions. Lines correspond to mean +/- SD of
847 technical replicates (*n*=3). **C)** HC single cell microscopy analysis of p62 puncta formation in BMDMs
848 transfected with scrbl or NRF2 siRNA and infected for 4 h with *L. interrogans* serovar Manilae strain
849 L495 at MOI 100. **D)** Corresponding controls are microscopy analyses and quantification of NRF2
850 intensity in the same transfection and infection conditions. Lines correspond to mean +/- SD of technical
851 replicates (*n*=3). **E)** WB of p62 in BMDMs transfected with scrbl or NRF2 siRNA and infected for 24 h
852 with *L. interrogans* serovar Manilae strain L495 at MOI 10 or 100. **F)** RT-qPCR analyses of p62 mRNA

853 levels in RAW264.7 cells transfected with scrbl or NRF2 siRNA and infected for 24 h with
854 *L. interrogans* serovar Manilae strain L495 at MOI 100. Bars correspond to mean of independent
855 experiments (*n*=2). **A-E)** Data presented are representative of at least 3 independent experiments.

856 **Figure 7. NRF2 translocation prevents inflammation upon infection**

857 **A)** Cell viability (measured by MTT assay) and **B)** LDH release (measured by CyQuant assay) in
858 RAW264.7 cells transfected with scramble (scrbl) or NRF2 siRNA and infected for 24 h with
859 *L. interrogans* serovar Manilae strain L495 at MOI 100. Bars correspond to mean +/- SD of technical
860 replicates (*n*=4). **B)** RT-qPCR analyses of iNOS, IL6, TNF and IL10 mRNA levels in RAW264.7 cells
861 transfected with scrbl or NRF2 siRNA and infected for 10 h with *L. interrogans* serovar Manilae strain
862 L495 at MOI 100. Bars correspond to mean of independent experiments (*n*=3). **C)** NO dosage by Griess
863 reaction and, IL6, TNF and IL10 by ELISA in RAW264.7 cells transfected with scrbl or NRF2 siRNA
864 and infected for 24 h with *L. interrogans* serovar Manilae strain L495 at MOI 100. Bars correspond to
865 mean +/- SD of technical replicates (*n*=4). **A-C)** Data presented are representative of at least 3
866 independent experiments.

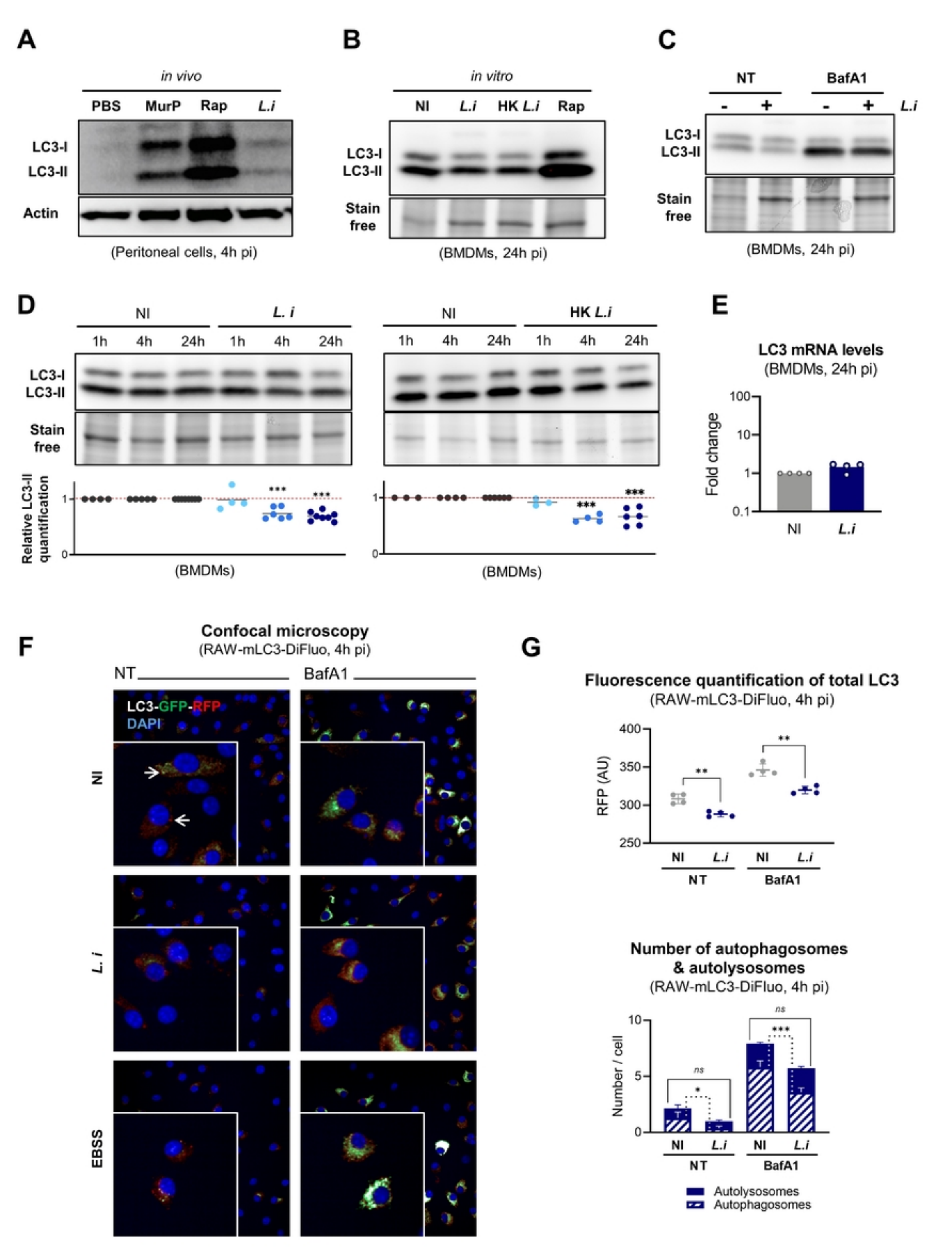
A
in vivo
PBS
MurP
Rap
L.i
LC3-I
LC3-II
Actin
(Peritoneal cells, 4h pi)
B
in vitro
NI
L.i
HK L.i
Rap
LC3-I
LC3-II
Stain free
(BMDMs, 24h pi)
C
NT
BafA1
-
+
-
+
L.i
LC3-I
LC3-II
Stain free
(BMDMs, 24h pi)
D
NI
L. i
1h
4h
24h
1h
4h
24h
LC3-I
LC3-II
Stain free
Relative LC3-II quantification
***
***
(BMDMs)
NI
HK L.i
1h
4h
24h
1h
4h
24h
***
***
(BMDMs)
E
LC3 mRNA levels
(BMDMs, 24h pi)
Fold change
100
10
1
0.1
NI
L.i
F
Confocal microscopy
(RAW-mLC3-DiFluo, 4h pi)
NT
BafA1
LC3-GFP-RFP
DAPI
NI
L. i
EBSS
G
Fluorescence quantification of total LC3
(RAW-mLC3-DiFluo, 4h pi)
RFP (AU)
400
350
300
250
**
**
NI
L.i
NI
L.i
NT
BafA1
Number of autophagosomes & autolysosomes
(RAW-mLC3-DiFluo, 4h pi)
Number / cell
10
5
0
ns
*
ns
***
NI
L.i
NI
L.i
NT
BafA1
Autolysosomes
Autophagosomes

Figure1

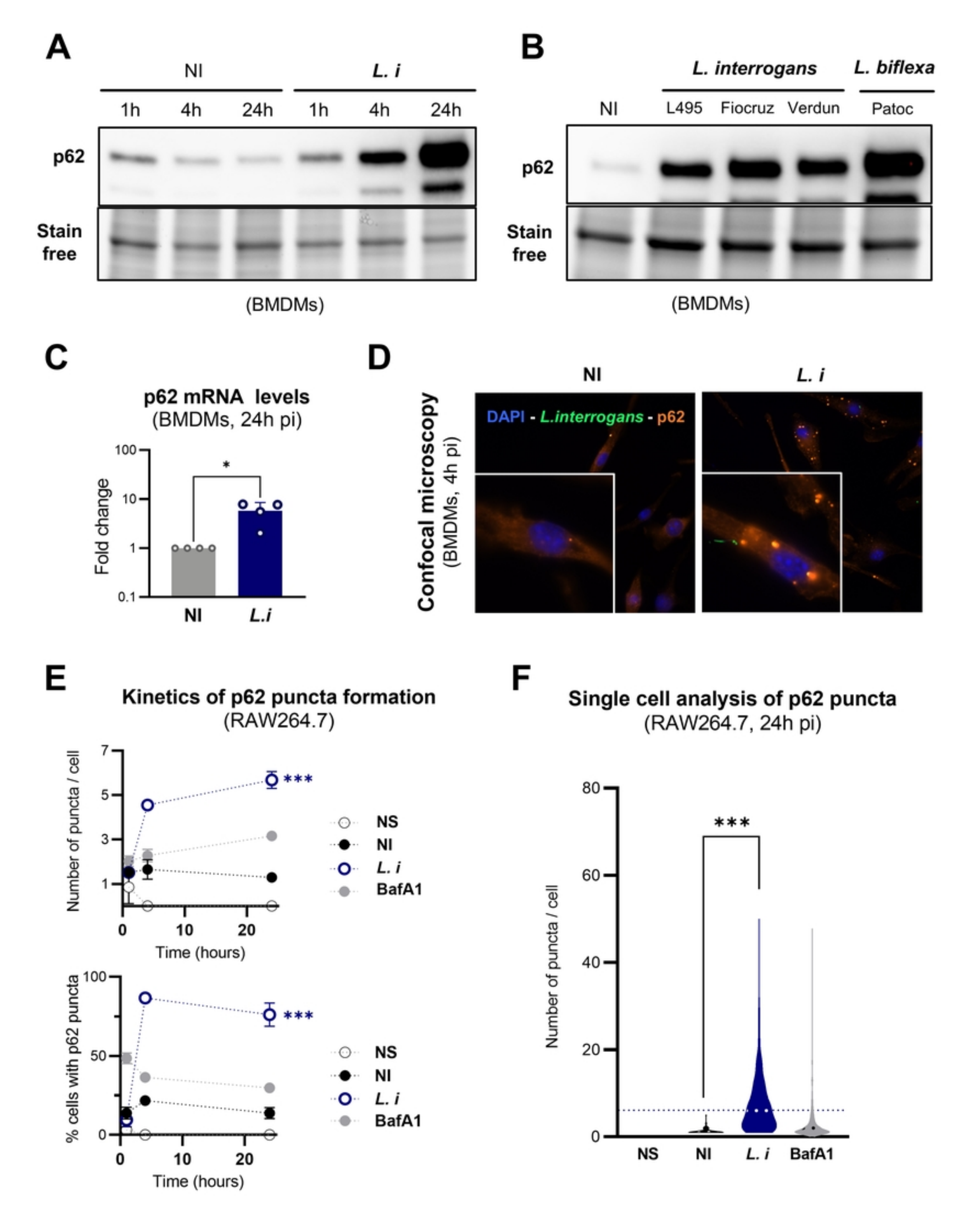
A
NI
L. i
1h
4h
24h
1h
4h
24h
p62
Stain free
(BMDMs)
B
L. interrogans
L. biflexa
NI
L495
Fiocruz
Verdun
Patoc
p62
Stain free
(BMDMs)
C
p62 mRNA levels
(BMDMs, 24h pi)
Fold change
100
10
1
0.1
*
NI
L.i
D
NI
L. i
Confocal microscopy
(BMDMs, 4h pi)
DAPI - L.interrogans - p62
E
Kinetics of p62 puncta formation
(RAW264.7)
Number of puncta / cell
7
5
3
1
***
0
10
20
Time (hours)
NS
NI
L. i
BafA1
% cells with p62 puncta
100
50
0
***
0
10
20
Time (hours)
NS
NI
L. i
BafA1
F
Single cell analysis of p62 puncta
(RAW264.7, 24h pi)
Number of puncta / cell
80
60
40
20
0
***
NS
NI
L. i
BafA1

Figure 2

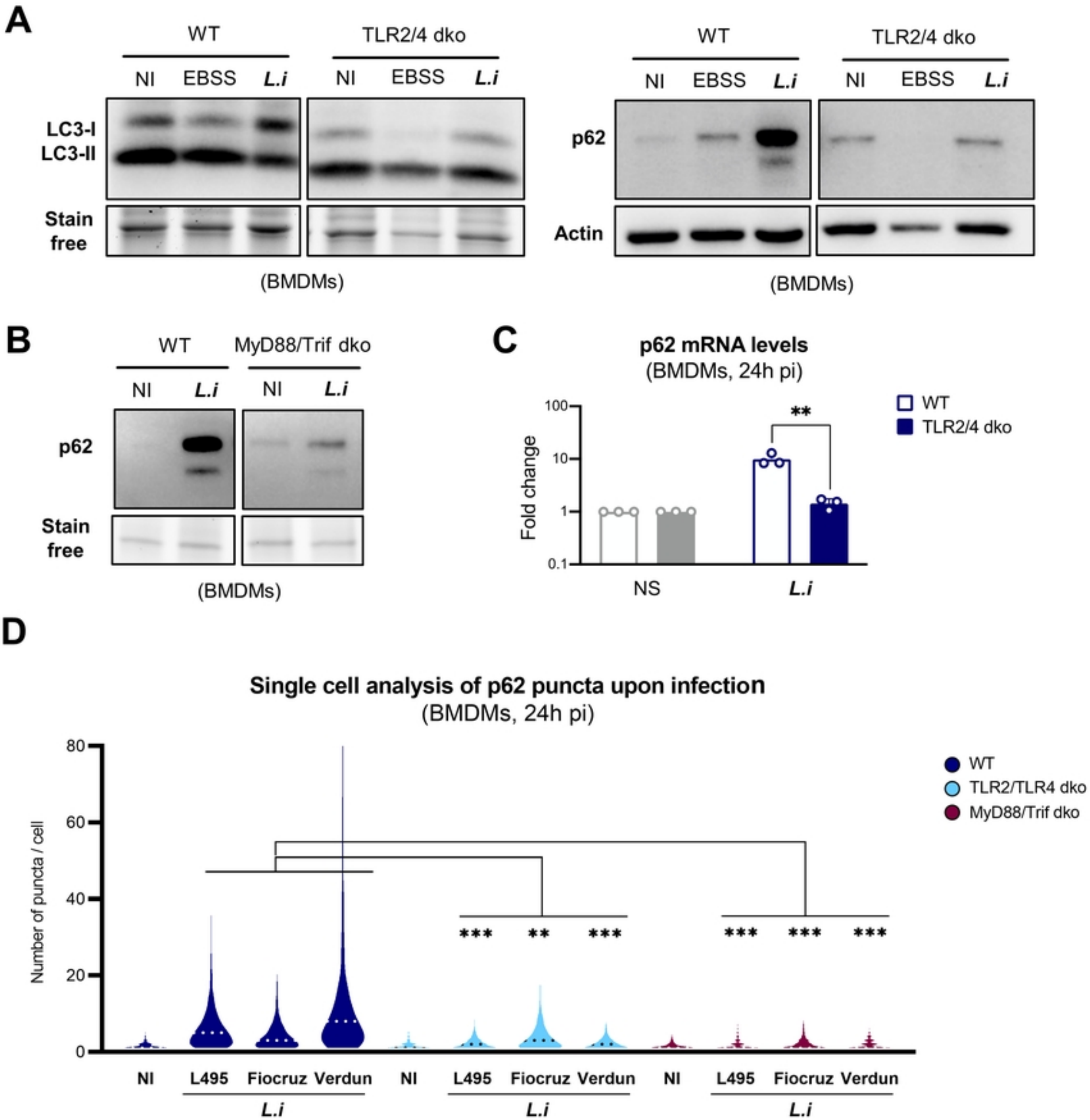
A
WT
TLR2/4 dko
NI
EBSS
L.i
LC3-I
LC3-II
Stain free
(BMDMs)
p62
Actin
B
MyD88/Trif dko
C
p62 mRNA levels
(BMDMs, 24h pi)
Fold change
100
10
1
0.1
**
NS
D
Single cell analysis of p62 puncta upon infection
(BMDMs, 24h pi)
Number of puncta / cell
80
60
40
20
0
***
WT
TLR2/TLR4 dko
MyD88/Trif dko
L495
Fiocruz
Verdun

Figure 3

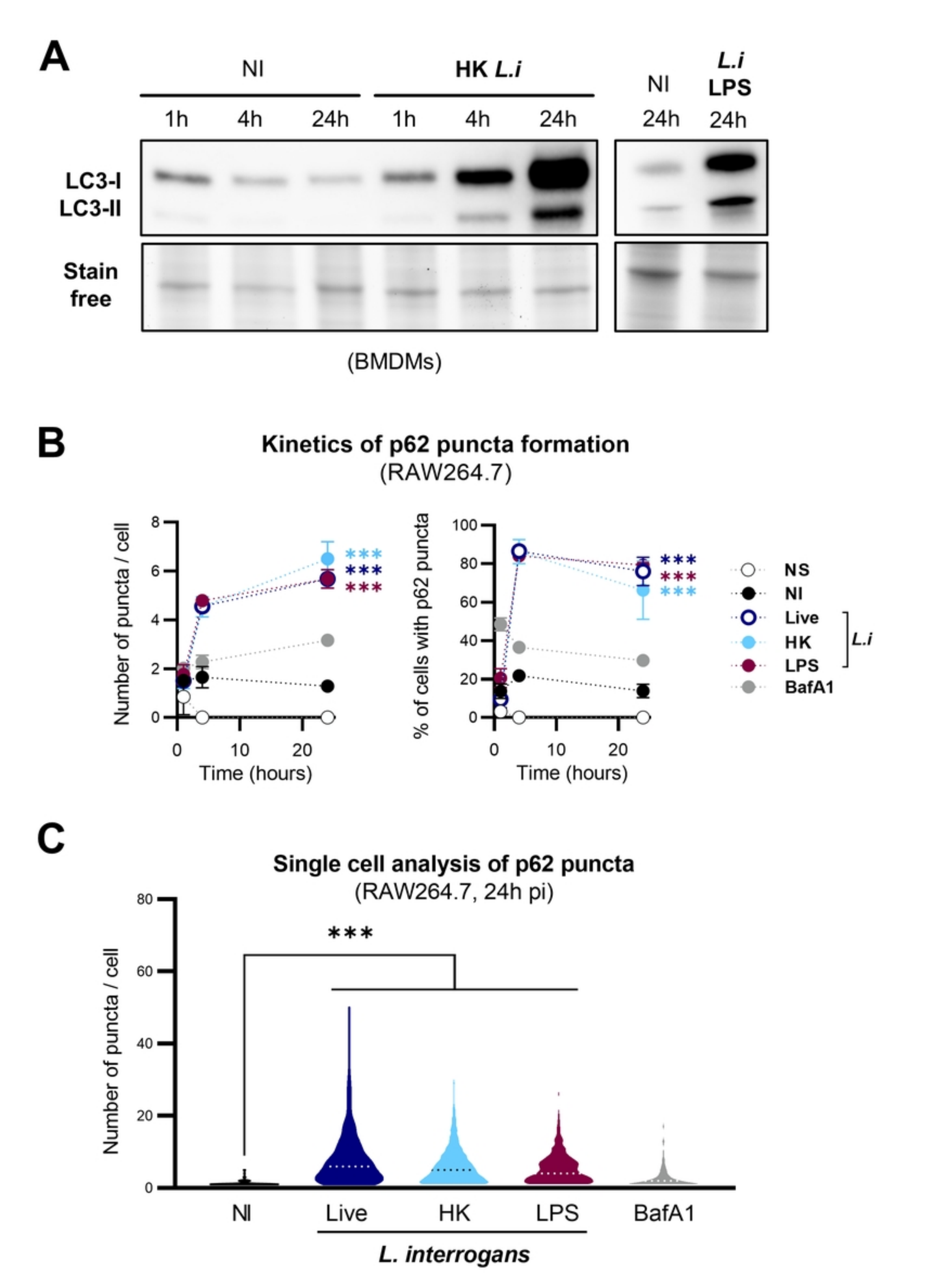
A
NI
HK L.i
NI
L.i LPS
1h
4h
24h
1h
4h
24h
24h
24h
LC3-I
LC3-II
Stain free
(BMDMs)
B
Kinetics of p62 puncta formation
(RAW264.7)
Number of puncta / cell
% of cells with p62 puncta
Time (hours)
Time (hours)
***
NS
NI
Live
HK
LPS
BafA1
L.i
C
Single cell analysis of p62 puncta
(RAW264.7, 24h pi)
Number of puncta / cell
***
NI
Live
HK
LPS
BafA1
L. interrogans

Figure 4

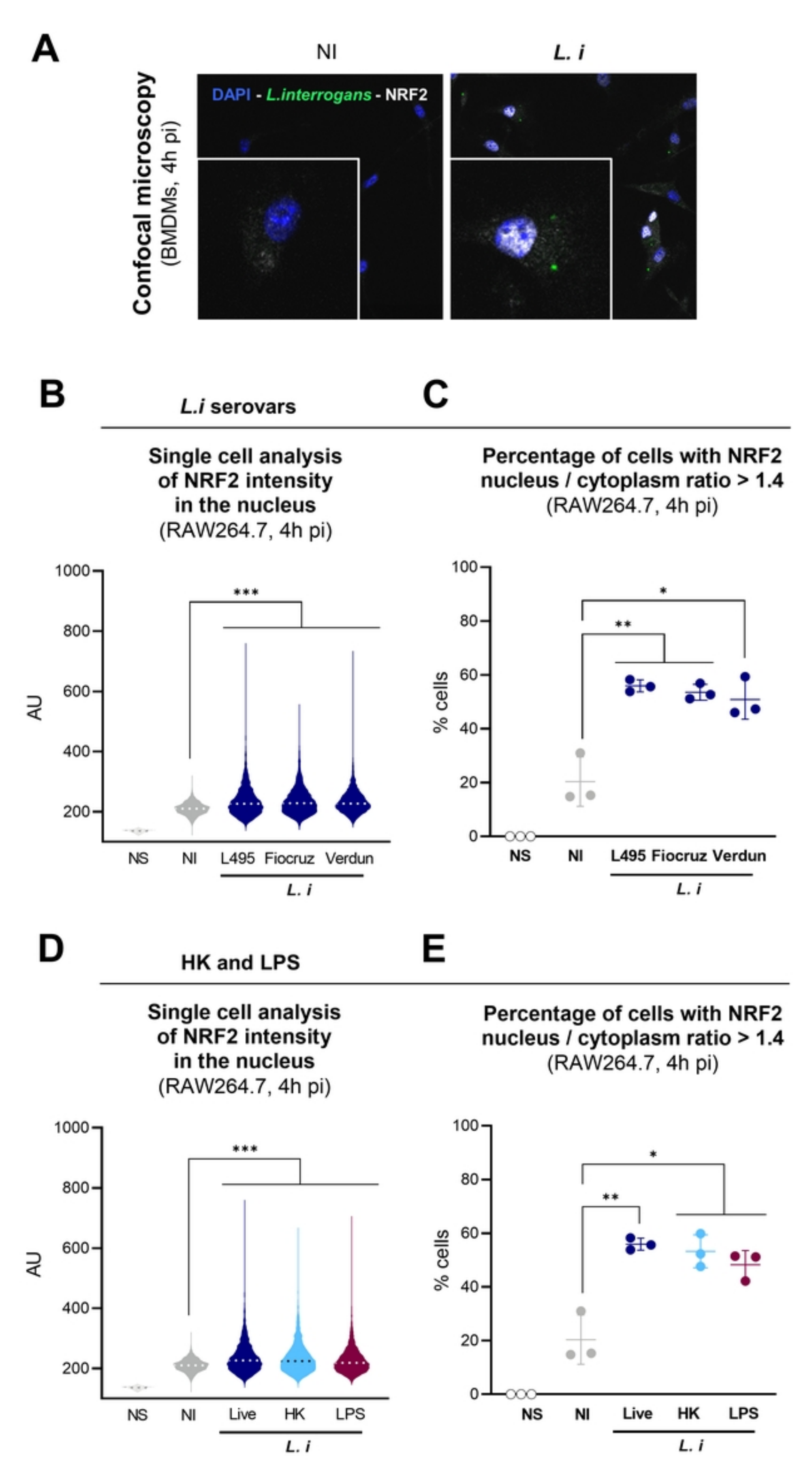
A
NI
L. i
Confocal microscopy
(BMDMs, 4h pi)
DAPI - L.interrogans - NRF2
B
L.i serovars
Single cell analysis
of NRF2 intensity
in the nucleus
(RAW264.7, 4h pi)
AU
1000
800
600
400
200
***
NS
NI
L495
Fiocruz
Verdun
L. i
C
Percentage of cells with NRF2
nucleus / cytoplasm ratio > 1.4
(RAW264.7, 4h pi)
% cells
100
80
60
40
20
0
*
**
NS
NI
L495
Fiocruz
Verdun
L. i
D
HK and LPS
Single cell analysis
of NRF2 intensity
in the nucleus
(RAW264.7, 4h pi)
AU
1000
800
600
400
200
***
NS
NI
Live
HK
LPS
L. i
E
Percentage of cells with NRF2
nucleus / cytoplasm ratio > 1.4
(RAW264.7, 4h pi)
% cells
100
80
60
40
20
0
*
**
NS
NI
Live
HK
LPS
L. i

Figure 5

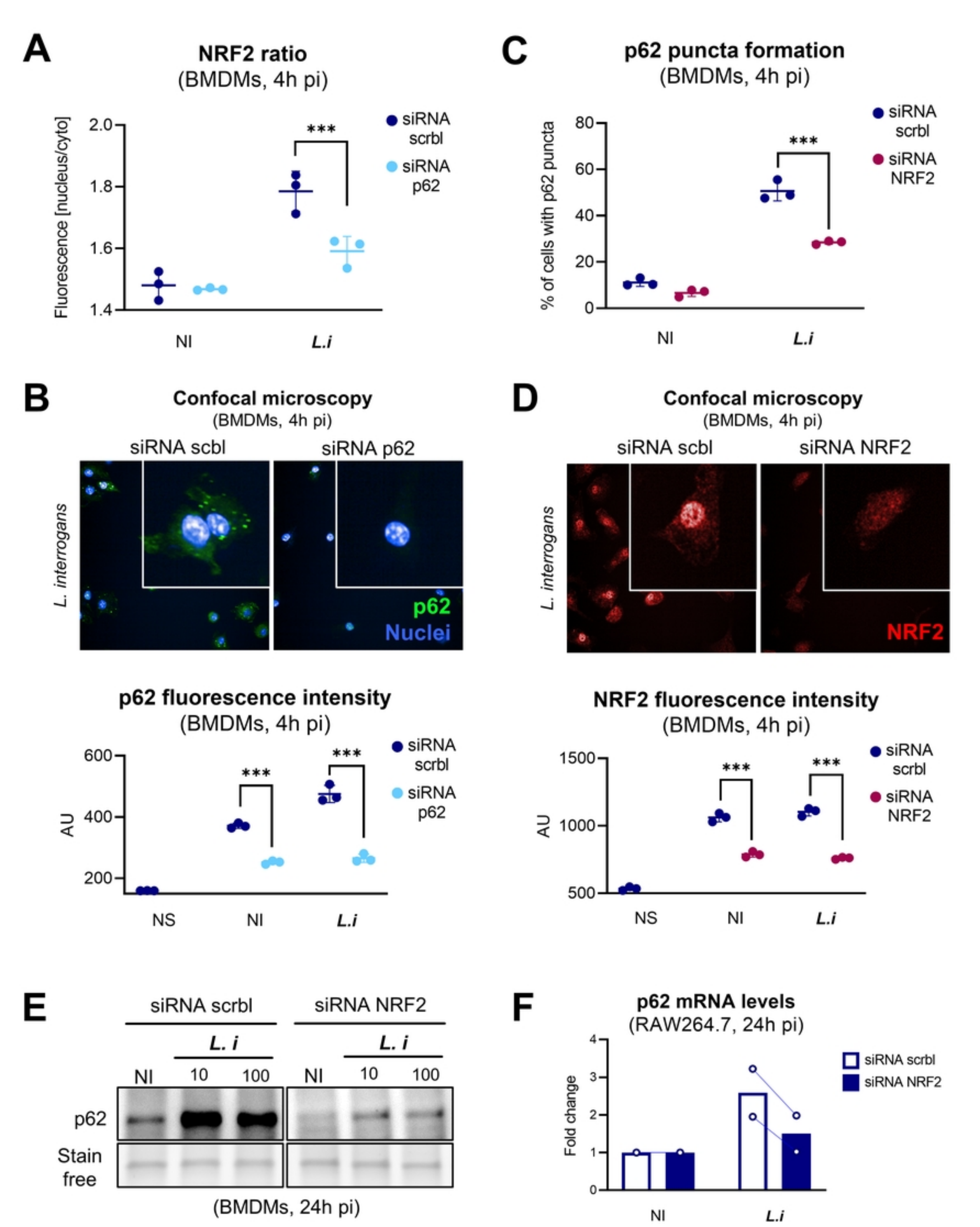
A
NRF2 ratio
(BMDMs, 4h pi)
Fluorescence [nucleus/cyto]
2.0
1.8
1.6
1.4
***
siRNA scrbl
siRNA p62
NI
L.i
C
p62 puncta formation
(BMDMs, 4h pi)
% of cells with p62 puncta
80
60
40
20
0
***
siRNA scrbl
siRNA NRF2
NI
L.i
B
Confocal microscopy
(BMDMs, 4h pi)
siRNA scbl
siRNA p62
L. interrogans
p62
Nuclei
D
Confocal microscopy
(BMDMs, 4h pi)
siRNA scbl
siRNA NRF2
L. interrogans
NRF2
p62 fluorescence intensity
(BMDMs, 4h pi)
AU
600
400
200
***
***
siRNA scrbl
siRNA p62
NS
NI
L.i
NRF2 fluorescence intensity
(BMDMs, 4h pi)
AU
1500
1000
500
***
***
siRNA scrbl
siRNA NRF2
NS
NI
L.i
E
siRNA scrbl
siRNA NRF2
L. i
L. i
NI
10
100
NI
10
100
p62
Stain free
(BMDMs, 24h pi)
F
p62 mRNA levels
(RAW264.7, 24h pi)
Fold change
4
3
2
1
0
siRNA scrbl
siRNA NRF2
NI
L.i

Figure 6

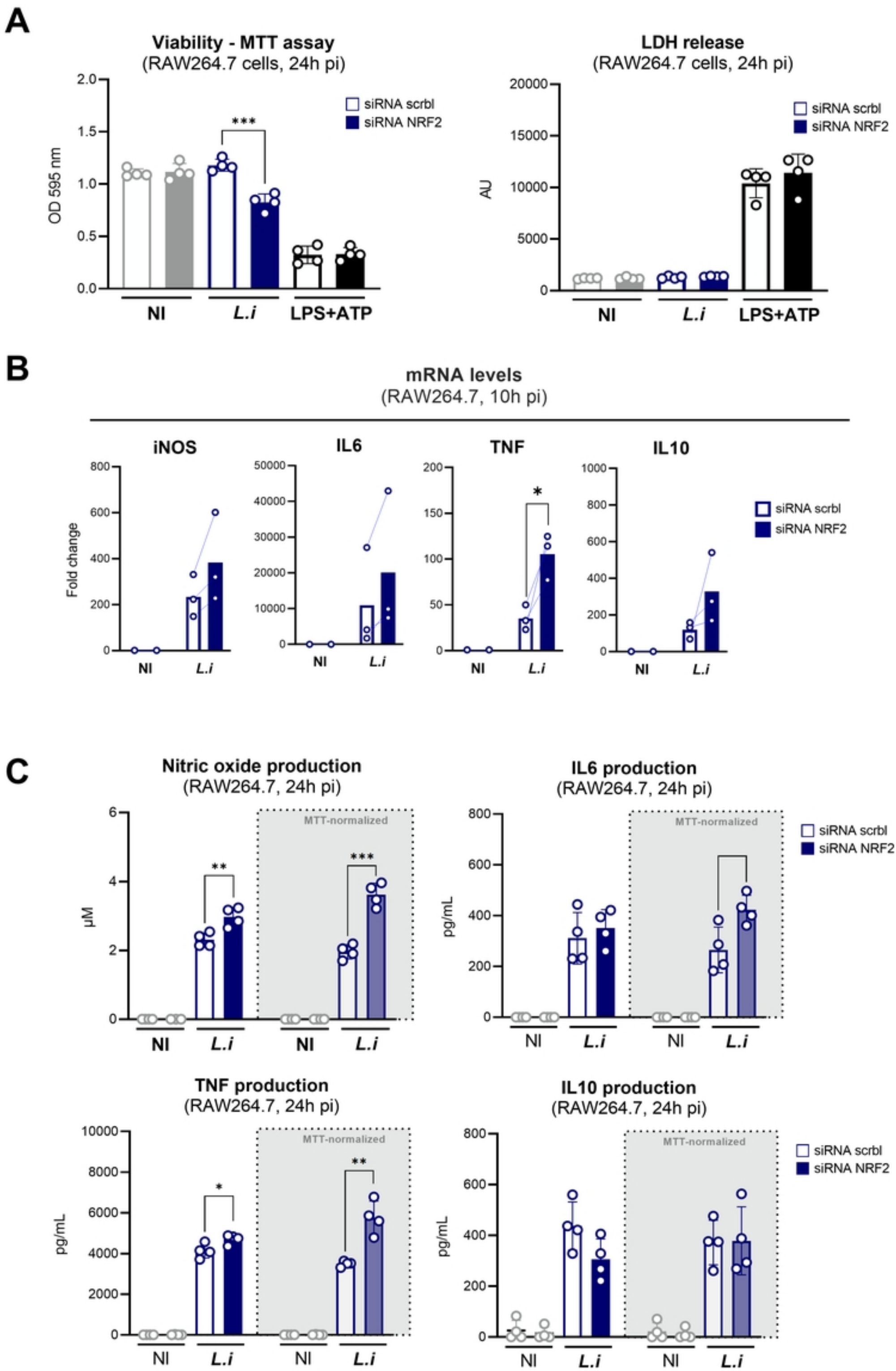
A
Viability - MTT assay
(RAW264.7 cells, 24h pi)
OD 595 nm
siRNA scrbl
siRNA NRF2
***
NI
L.i
LPS+ATP
LDH release
(RAW264.7 cells, 24h pi)
AU
B
mRNA levels
(RAW264.7, 10h pi)
iNOS
IL6
TNF
IL10
Fold change
*
C
Nitric oxide production
(RAW264.7, 24h pi)
μM
MTT-normalized
**
IL6 production
(RAW264.7, 24h pi)
pg/mL
TNF production
(RAW264.7, 24h pi)
IL10 production
(RAW264.7, 24h pi)

Figure 7